International Journal of Robotics and Control Systems
Vol. 6, No. 1, 2026, pp. 115-142
ISSN 2775-2658
http://pubs2.ascee.org/index.php/ijrcs

Wearable Extra Robotic Arms: Data-Driven Control for Supernumerary Robotics Arms

M. Munadi [a,1,*], Mochammad Ariyanto [a,2], Joga Dharma Setiawan [a,3], Dedy Mulyanto [a,4], Tanto Nugroho [a,5], Yoshiaki Taniai [b,6]

[a] Department of Mechanical Engineering, Faculty of Engineering, Universitas Diponegoro, Semarang, 50275, Indonesia
[b] Faculty of Education, Information Science, Yamaguchi University, Yamaguchi, 753-0841, Japan
[1] munadi@ft.undip.ac.id; [2] mochammad_ariyanto@ft.undip.ac.id; [3] joga.setiawan@ft.undip.ac.id;
[4] dmulianto@gmail.com; [5] tantonugroho94@gmail.com; [6] taniai@yamaguchi-u.ac.jp
* Corresponding Author

ARTICLE INFO

Article history
Received August 26, 2025
Revised October 15, 2025
Accepted December 26, 2025

Keywords
Wearable Extra Arms;
Cooperative Control;
Neural Network Control;
Wearable Robotics;
Human-Robot Cooperation

ABSTRACT

While extra robotic limbs hold promise for enhancing human capabilities through physical assistance, challenges persist in improving their effectiveness, cooperative control, safety, and overall user-friendliness. This study developed an integrated system using wearable extra robotic arms (ERAs), soft grippers, and glove sensor interfaces to enable shared control of complex cooperative manipulation tasks. Lightweight 4-DOF ERAs provided dexterous reaching assistance, while soft grippers employing pneumatic actuation permitted gentle object grasping. A customized sensor glove incorporating flex sensors and an inertial measurement unit (IMU) was applied to wirelessly measure the user's hand movements. A machine learning approach was implemented for coordinated control, in which the user's hand motion angles measured by the glove sensor drove the extra arms through a neural network model trained on paired human–robot arm data. The contribution of this work lies in embedding a lightweight neural network into a constrained microcontroller to achieve real-time proprioceptive mapping between the user's biological motion and the robotic limbs. This real-time biological–robotic arms mapping directed cooperative motions without explicit control programming or inverse kinematic computation. Seven multi-arm cooperative object manipulation tasks were conducted over repeated trials. The results confirm the feasibility of the proposed wearable extra robotic arms equipped with a machine-learning interface in assisting users with complex manipulation tasks that are challenging for a single person to perform.

1. Introduction

Supernumerary robotic limbs (SRLs) are a promising development in wearable robot technology. These additional robotic limbs can be attached to the body and provide mechanical assistance, augmenting human capabilities. Researchers have developed three main categories of SRLs: fingers, arms, and legs. Supernumerary robotic fingers (SRFs) are designed to work alongside biological hands or fingers. Mounted on the wrist, these robotic appendages typically possess one, two, or more fingers

that can be controlled through various interfaces like electromyography (EMG), flex or stretch sensors [1]-[6]. They offer additional grasping for a person with weakened hand function. Additionally, SRFs can enhance dexterity for healthy users, allowing them to manipulate objects in new ways or perform complex tasks with a single hand. Supernumerary robotic arms (SRAs) are an augmented technology that provides users/wearers with additional robotic arms. SRAs have been developed for various applications, such as increasing strength and dexterity for specific tasks in manufacturing or rehabilitation, as well as enhancing human manipulation tasks [7]-[13]. Supernumerary robotic legs function as extra appendages, providing additional degrees of freedom and mechanical assistance to the user's lower limbs. SRLs enhance human mobility in various applications such as standing/sitting assistance, balance augmentation, rehabilitation, and assisting the user in walking [14]-[20].

Developing supernumerary robotic limbs in extra fingers, arms, or legs presents diverse challenges that researchers must address to realize their full benefits and applications. One of the most challenging issues is creating intuitive control interfaces that enable seamless communication between the human biological and additional robotic limbs. Achieving smooth coordination and cooperation between these extra robotic limbs and natural biological ones is also crucial in preventing undesirable movements. Despite extensive progress, most SRL systems still face significant challenges in relying on high-dimensional bioelectric sensor signal processing [21]-[24] or computationally intensive inverse kinematics [25]-[28].

A crucial challenge in SRAs or extra robotic arms lies in developing intuitive control interfaces. Unlike traditional prosthetics that replace limbs, SRLs introduce entirely new appendages, demanding novel and intuitive control methods [29]-[33]. Ideally, the control should mimic natural human movement for seamless integration. One promising approach explores mimicking biological signals and translating muscle activity or brain-computer interfaces into commands for the SRLs.

Electromyography (EMG) sensors, which measure electrical activity in muscles, offer a promising approach to this challenge as the input sensor for the SRAs. By decoding EMG signals from the user's limbs or healthy muscles, machine learning can translate the user's intended movements into commands [15], [16], [34], [35]. This approach has the potential to create a more natural and intuitive user experience compared to simple traditional control methods such as analog joysticks or switches. An electroencephalography (EEG) sensor offers a non-invasive method for capturing brain activity, potentially allowing users to control SRLs through their thoughts. By decoding specific EEG patterns associated with movement intention, researchers aim to create a direct link between the user's brain and the SRL via the EEG signal recognition method [12], [36]-[38]. This approach holds promise for creating a more natural and intuitive control interface. However, they present distinct challenges. EEG can be susceptible to user fatigue, external noise interference, and limitations in precise movement control. Conversely, EMG, relying on muscle signals, faces difficulties in isolating specific muscle activation from complex movements, especially when controlling and cooperating with multiple extra robotic arms simultaneously with a higher degree of freedom. Additionally, both sensors and the user's intention recognition method require significant data training and complex computation to achieve the optimal control accuracy.

An alternative approach for controlling the SRLs involves augmenting the use of an Inertial Measurement Unit (IMU) or other body-mounted sensors with machine learning algorithms/other control systems [39]. IMUs track the wearer's body movements and orientation, providing signals that can be interpreted by machine learning models to predict the user's intended actions. This approach offers several advantages. Unlike EMG or EEG, IMU-based control is less susceptible to user fatigue or external noise. Additionally, IMU can capture broader movement patterns, potentially simplifying control for multi-arm robots. By learning and adapting to the user's specific movement patterns, machine learning algorithms can refine control over time, leading to a more intuitive and natural user experience. Yet, most IMU-based SRLs rely on extensive computation, control, or kinematic mapping.

To address these gaps, this study introduces a fully embedded, data-driven control framework for wearable extra robotic arms (ERAs) that performs real-time proprioceptive mapping between human

and robotic limbs directly on a constrained microcontroller. The proposed system integrates a lightweight 4-DOF ERA augmented with soft pneumatic grippers for gentle object manipulation. A custom-designed sensor glove equipped with flex sensors and an IMU captures the user's hand postures as proprioceptive inputs. Using paired datasets of human and the ERA movements, a neural network model was trained to map these proprioceptive signals into synchronized servo motor commands for coordinated multi-joint motions of the extra arms. The contribution of this work lies in embedding a lightweight neural network entirely within a low-power microcontroller, enabling fully onboard, real-time coordination without extensive computation, inverse kinematics, or high-dimensional bioelectric sensing. The system was tested through seven complex cooperative manipulation tasks, demonstrating effective shared biological–artificial coordination control for activities that are difficult to perform by a single person.

2. Method

2.1. Extra Robotic Arms (ERA) System

The ERA developed in this study featured a lightweight yet robust design with four degrees of freedom for dexterous manipulation. The structural components were constructed from aluminum to achieve a strength-to-weight ratio suitable for the coordination of object manipulation assistance. Actuation was provided by servo motors (RDS3135) capable of generating up to 35 kg.cm of maximum torque, located at each of the arm's four joints. A vest system was utilized to securely mount both left and right extra robotic arms, as well as their accompanying control electronics / electronic backpack, directly to the user's torso via a vest jacket. This wearable configuration allowed for the integration of the assistive technology with the human body during cooperative tasks. The total length of each ERA is 650 mm, and the total weight of both ERAs, including the controller box, vest jacket, and soft gripper, is 2.8 kg.

The controller consisted of two Arduino Mega controllers for independently controlling each ERA, along with two mini compressors, four mini solenoid valves, and a battery. All electronics were mounted within a box that was integrated into a wearable vest jacket. This configuration allowed a user to easily wear and remove both the assisted ERAs and their accompanying controller simply by putting on or taking off the single vest unit. The vest thereby provided a means of portable integration for the complete assistive technology system. A three-fingered soft robotic gripper, designed for gentle and adaptive grasping of various objects, was affixed to the end of each ERA. This gripper provided the necessary end-effector functionality for tasks involving assistive object manipulation interaction. The proposed system for both ERAs is presented in Fig. 1, and the result of the ERA prototype worn by a user is shown in Fig. 2.

Forward kinematics was applied to analyze the ERA movement. The end-effector of the robotic arm's position can be calculated based on the angles of its joints. This relationship is expressed as a function using position and orientation parameters. Position parameters define the robot's location in space, while orientation parameters specify the coordinate frame at each joint. The proposed ERA has four coordinate frames on the left or right. The forward kinematics focuses on analyzing the arm's movement without the gripper attached. The Denavit-Hartenberg (DH) parameters were derived from the initial positions of the robotic arms as shown in Supplementary Information Fig. 11. The DH parameters of ERA are summarized as written in Table 1. Each ERA has two links and four joints on both the right and left sides.

Forward kinematics analysis relies on homogeneous transformation matrices to map the relationship between joint rotations (servo angle input) and end-effector pose. For the extra robotic arm with four degrees of freedom, the relevant transformation is defined from the base frame (frame 0) to the end-effector frame (frame 3). This transformation is mathematically described by Equation (1). Performing this calculation using the DH parameters produces an equation to determine the XYZ coordinates of the end-effector. These coordinates represent the position and orientation of the artificial limb tip as a function of each joint angle. The input to drive these joint angles is written in Equation (2), which relates the servo motor angles to the revolute joints of the robotic arm. Therefore,

by combining Equations (1) and (2), the forward kinematics analysis provides an explicit relationship between low-level servo commands and the resulting high-level arm posture achievable through motion coordination with the user's hand posture.

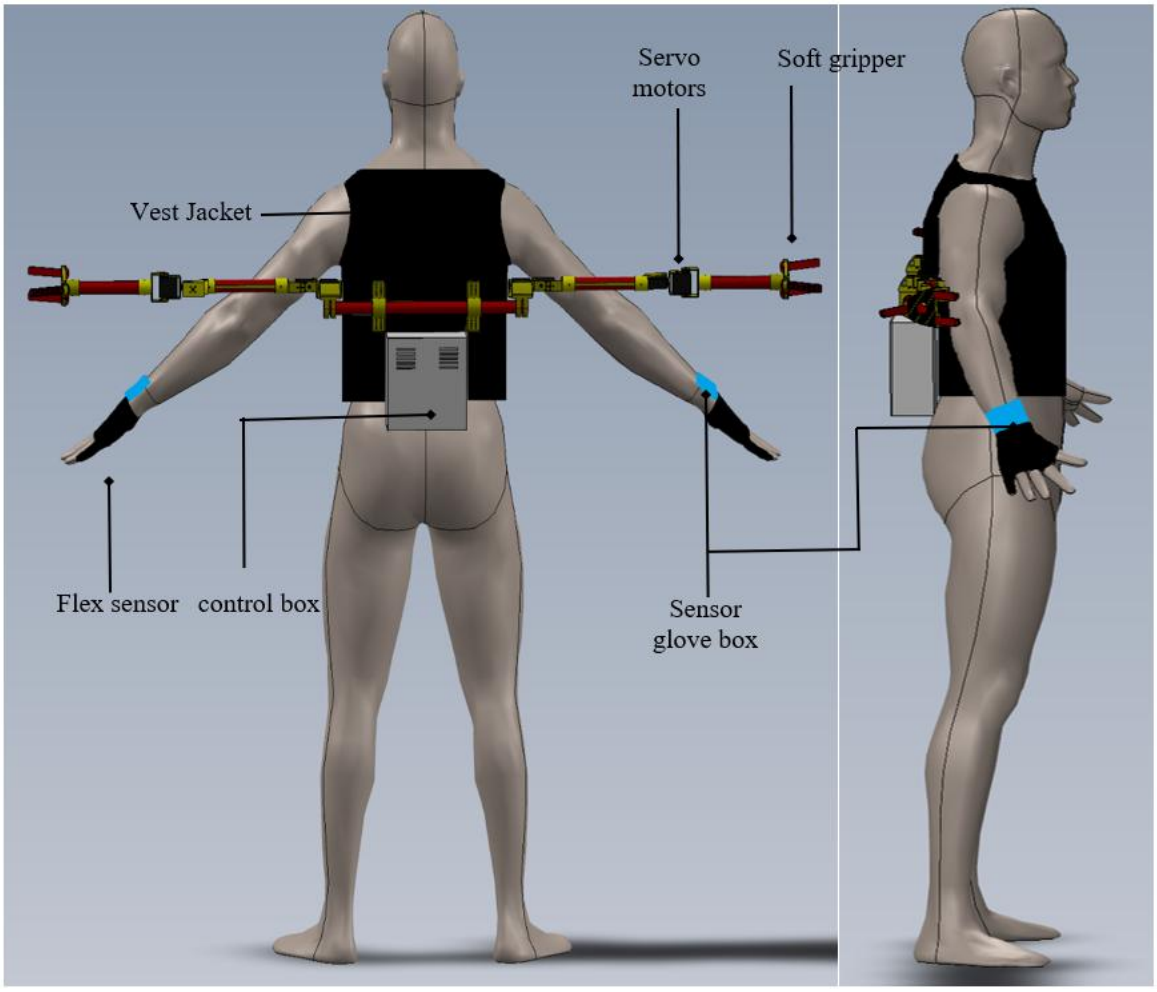

Fig. 1. Overview of the proposed wearable extra robotic arm system featuring dual 4-DOF arms with soft grippers, a vest-mounted controller unit, and a sensor glove enabling coordinated control. The result of the extra arms augmented with soft grippers can be seen in Supplementary Video S1 (https://bit.ly/43Zz36I).

$$T = \prod_{n=1}^{4} = \begin{bmatrix} cos\,\theta_i & -sin\,\theta_i \cdot cos\,\alpha_i & sin\,\theta_i \cdot sin\,\alpha_i & a_i\,cos\,\theta_i \\ sin\,\theta_i & cos\,\theta_i \cdot cos\,\alpha_i & -cos\,\theta_i \cdot sin\,\alpha_i & a_i\,sin\,\theta_i \\ 0 & sin\,\alpha_i & cos\,\alpha_i & d_i \\ 0 & 0 & 0 & 1 \end{bmatrix} \quad (1)$$

$$\begin{aligned} X &= 0.302\,cos\,\theta_1\,sin\,\theta_2 - 0{,}227\,cos\,\theta_4\,(sin\,\theta_1\,sin\,\theta_3 - cos\,\theta_1\,cos\,\theta_2\,cos\,\theta_3) + 0.227\,cos\,\theta_1\,sin\,\theta_2\,sin\,\theta_4 \\ Y &= 0.302\,sin\,\theta_1\,sin\,\theta_2 + 0.227\,cos\,\theta_4\,(cos\,\theta_1\,sin\,\theta_3 + cos\,\theta_2\,cos\,\theta_3\,sin\,\theta_1) + 0.227\,sin\,\theta_1\,sin\,\theta_2\,sin\,\theta_4 \\ Z &= 0.302\,cos\,\theta_2 + 0.227\,cos\,\theta_2\,sin\,\theta_4 - 0.227\,cos\,\theta_3\,cos\,\theta_4\,sin\,\theta_2 + 0.038 \end{aligned} \quad (2)$$

The proposed ERA aimed to achieve coordinated control by mimicking the user's natural movements. A key component was a glove equipped with flex sensors and an IMU. The flex sensors (2.2" 10K Flexible Sensor) measured finger bending, and the IMU (MPU-9150) estimated roll and pitch angles. This wireless hand posture and motion measurement in real-time was wirelessly transmitted to the ERA controller via a 2.4GHz radio module, as shown in Fig. 2.

On the ERA controller, a neural network model translated the user's hand angles (roll and pitch) into commands for the robotic arm's servo motors. This system mirrored the user's biological hand

motion, creating a mapping between hand posture (roll and pitch) and arm movement for coordination control between the biological arm and the robotic arm. By implementing a wireless feedback mechanism and coordinated control scheme based on the neural network mapping of joint angles, the system allowed the ERA to be coordinated directly with the natural posture of the user's hands. This synchronous coordination capability empowered a user/wearer to be assisted in completing complex physical manipulation tasks that would be difficult for a single person. Fig. 2 depicts the design and implementation of wearable extra robotic arms (ERAs). Fig. 2 a illustrates the communication architecture block for each ERA, outlining the data flow between sensors, the main controller, and actuators. The electronic circuitry of the extra arm is detailed in Fig. 2 b. Finally, Fig. 2 c presents a photograph showcasing an ERA and the accompanying glove sensor during actual use by a user/wearer.

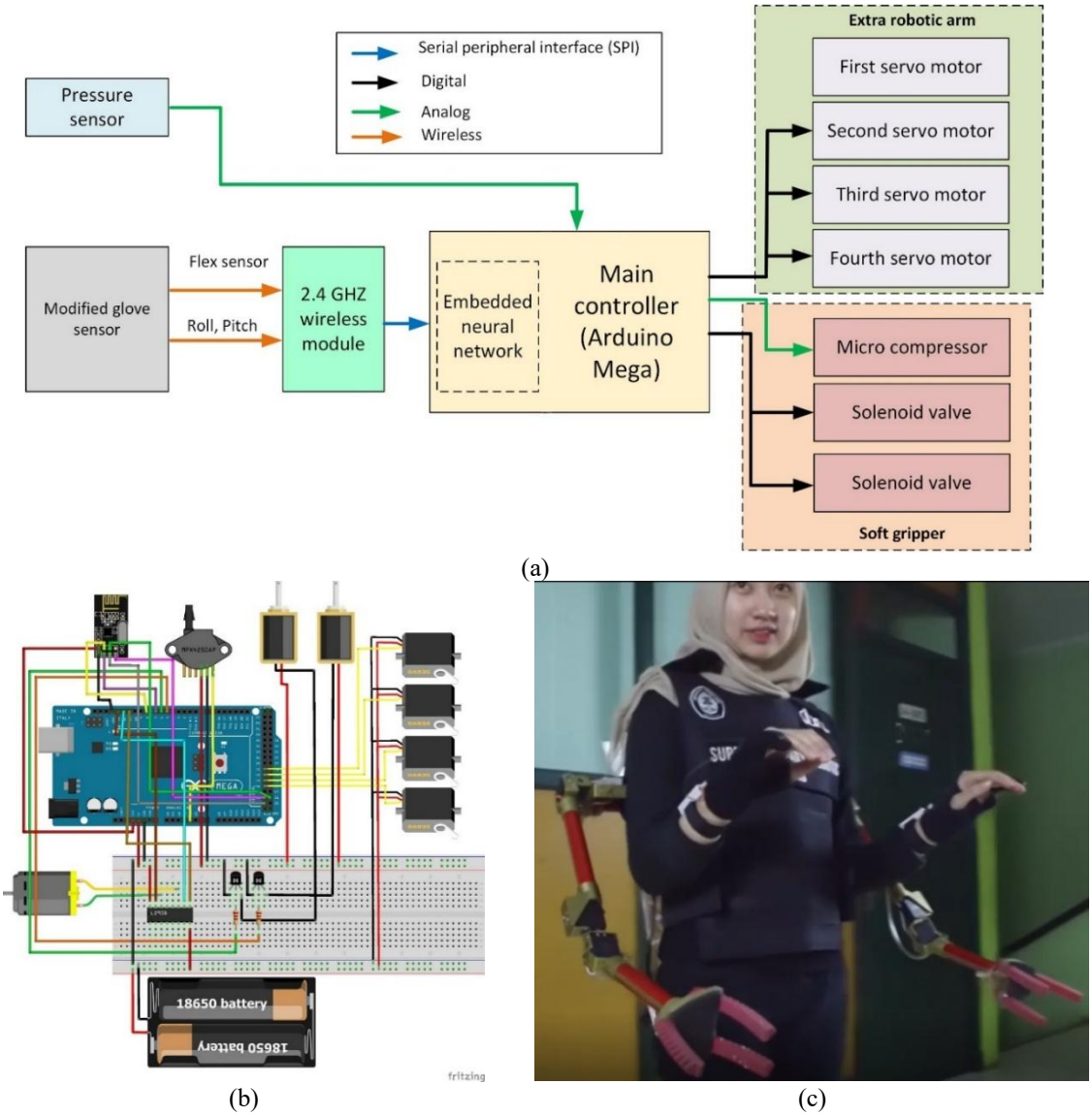

Fig. 2. Wearable Extra robotic arms. (a) Communication diagram block for each ERA (left and right) among sensors, the main controller, and actuators. (b) Electronic wiring diagram of the extra arm. (c) Photograph of the ERA and the glove sensor when it was worn by a user

A pneumatic network-based soft robotic gripper was chosen as the end effector of the ERA to grasp the objects. It offers dexterous manipulation due to its inherent compliance and adaptability. It leverages the power of compressed air to actuate soft, flexible materials, enabling gentle and secure grasping of objects with varying shapes and sizes [40]-[44]. A soft robotic gripper employing pneumatic actuation was designed and fabricated for this study. From a mechanical design

perspective, the gripper incorporated three main components as illustrated in Fig. 4 a. Specifically, the soft finger material was selected as RTV-52 silicone rubber due to its compliant and flexible nature, suitable for delicate grasping. Each finger consisted of a single continuous strip of the soft pneumatic material. Accompanying the flexible fingers was a gripper housing and fixator system. The housing, 3D printed from poly lactic acid (PLA) resin, served to anchor the soft finger actuators and guide their movement during inflation/suction and deflation/discharge. A fixator lock was also utilized to securely fasten each finger to the housing interior while still permitting deformation.

Table 1. DH parameters for the left/right extra arms

Joint	d_i (m)	a_{i-1} (m)	α_{i-1} (deg)	θ_i
1	0.038	0	-90	θ_1
2	0	0	90	θ_2
3	0.302	0	90	θ_3
4	0	0.227	0	θ_4

Pneumatic actuation was applied to enable the bending motion of the soft robotic gripper. Mimicking biological muscle-tendon systems, it provided a means of soft, flexible actuation that was suitable for grasping delicate and fragile objects. The proposed soft gripper system incorporated a mini air compressor, solenoid valves, and interconnecting tubing. The compressor pressurized air, which was then routed through a distribution system of solenoid valves. This pneumatic network architecture allowed for both inflation and deflation processes of the soft gripper fingers to bend, as presented in Supplementary Information Fig. 12. By controlling airflow into and out of the silicone finger actuators via the solenoid valves, the gripper was able to dynamically transition between positive and negative pressure states.

2.2. Sensor Glove

Supernumerary robotic arms/legs/fingers utilize various sensors to achieve coordinated movements commanded by a user/wearer. These sensors can be attached to a user's body, most commonly on the hands, feet, or head, depending on the intended function of the extra arms. This integration allows the sensors to measure a biological signal such as muscle activity or human limb movement, enabling the supernumerary arms to respond naturally to the user's intentions. To aid in complex two-handed tasks, researchers employed stretch sensors and flex sensors attached to human fingers [4]-[6], [45]. These sensors captured finger movements or finger bending, which were then fed into a controller/machine learning for processing the measured finger movement. This allowed the controller to hold and manipulate objects for bimanual tasks that would be challenging with just one hand.

SRLs can be controlled intuitively using EMG sensors. By processing the EMG signals with digital signal processing and machine learning recognition, the system can decode the intended movements and translate them into commands for the extra robotic limbs [3], [46]-[48]. Force sensors are mounted on the extra robotic limbs, typically at the tips of the gripper/limb or contact points with the environment. These sensors measure the forces exerted by the extra robotic limb during interaction with the object [4], [9], [10], [49], [50]. Force sensor feedback plays a vital role in making supernumerary robotic limbs more intuitive and safer for various grasping and manipulation applications.

IMUs show potential for the control of supernumerary robotic limbs. IMUs typically contain gyroscopes and accelerometers that can provide critical orientation and movement data without external tracking systems. This intrinsic sensing makes IMUs well-suited for robotic limbs meant to interact directly with the user. By placing the IMU sensor at the joint of extra robotic arms, the posture and motion of the artificial limb can be estimated in real-time by fusing the measured gyroscope, accelerometer, and magnetometer. IMU feedback allows the extra robotic arm to seamlessly

coordinate with the user's motions and intentions [2], [7], [8], [51]-[53]. However, IMU measurement comes with challenges. Sensor drift over time introduces noise and errors that decrease the accuracy of the measurement. To counter this drift, some techniques like the Kalman filter and machine learning can correct the estimated measurement [54], [55].

This study developed a custom-modified glove system to capture the user's hand movement and little finger gestures. A Flex sensor was used to measure finger bending as input for controlling a soft robotic gripper. The Flex sensors also helped secure an extra robotic arm in customized assistive holding postures during object manipulation tasks. An IMU containing a 3-axis accelerometer and 3-axis gyroscope was selected to measure the angular motion of the user's hand. Attitude angles were estimated through a custom IMU filter implemented on an Arduino Nano controller. This allowed the computation of estimated attitude angles directly on the sensor glove controller. The filter was embedded into the glove controller via the Simulink Support Package for Arduino Hardware. By combining the flex sensor and IMU inputs mounted on the sensor glove box, the custom glove system was able to capture both the angular position and movement of the user's hands and fingers to enable coordinated control of assistive robotic limbs.

Wireless communication between the glove sensor system and the extra robotic arm controller was enabled through a 2.4 GHz nRF24L01 module. As shown in Fig. 3 a and Fig. 3 b, this module transmitted both the flex sensor measurements of finger bending motion and the estimated attitude angles from the IMU. Fig. 3 a depicts the sensor communication block diagram, showing how data was sent wirelessly from the Arduino Nano on the glove to the main controller of the extra robotic arm. Fig. 3 b provides the wiring diagram to illustrate how the sensors and wireless module were integrated into the glove's circuitry. The fully developed wearable glove prototype, as worn by a user, is pictured in Fig. 3 c. With the wireless transmission of proprioceptive data via the nRF24L01 module, the custom glove system allowed wireless communication between the operator's natural hand movements and an assisted extra robotic limb in real-time.

In this study, the orientation (Euler angle) estimated by the modified glove sensor was calculated based on 3-axis accelerometers and 3-axis gyroscope. Madgwick Filter [56] was selected to estimate the glove orientation with a simpler algorithm consisting of sensor fusion from the accelerometer and gyroscope. The filter implemented a quaternion representation to avoid singularities in 3D space for estimating the orientation [56], [57]. The quaternion can be represented as written in Equation (3).

$$q = [q_0 \quad q_1 \quad q_2 \quad q_3]^T \tag{3}$$

The acceleration vector is measured by 3-axis accelerometer and the norm of the measured acceleration vector can be calculated using Equation (4).

$$\begin{bmatrix} a_{x_n} \\ a_{y_n} \\ a_{z_n} \end{bmatrix} = \frac{1}{\sqrt{a_{x^2} + a_{y^2} + a_{z^2}}} \begin{bmatrix} a_x \\ a_y \\ a_z \end{bmatrix} \tag{4}$$

The field from the gravitational direction (v_x, v_y, *and* v_x) can be estimated using quaternions as written in Equation (5).

$$\begin{bmatrix} v_x \\ v_y \\ v_z \end{bmatrix} = \begin{bmatrix} 2(q_1 q_3 - q_0 q_2) \\ 2(q_0 q_1 - q_2 q_3) \\ q_0 q_0 - q_1 q_1 - q_2 q_2 + q_3 q_3 \end{bmatrix} \tag{5}$$

Error is the number of cross products between the reference direction of the gravitational field (v_x, v_y, v_z) and the direction measured by the accelerometer sensor (a_x, a_y, *and* a_z) as written in Equation (6).

$$\begin{bmatrix} e_x \\ e_y \\ e_z \end{bmatrix} = \begin{bmatrix} v_y a_z - v_z a_y \\ v_y a_z - v_z a_y \\ e_z = v_x a_y - v_y a_x \end{bmatrix} \tag{6}$$

Adjusted gyroscope estimated measurements can be calculated with a formula using the error value of the vector accelerometer with a proportional-integral (PI) compensator, as shown in Equation (7). The selected *Kp* and *Ki* are 100 and 0.02, respectively.

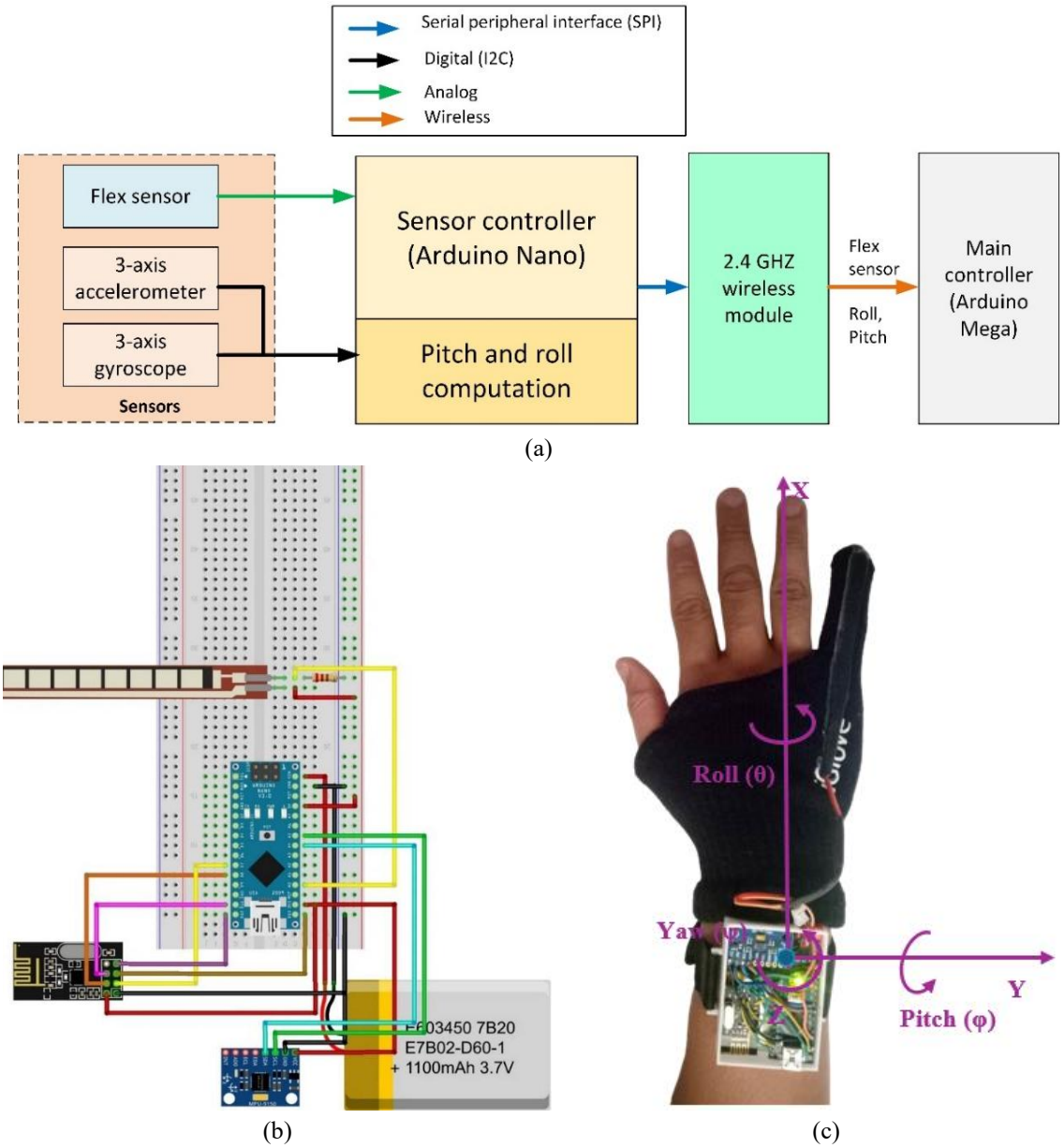

Fig. 3. Proposed modified soft glove sensor. (a) Block diagram of the communication system on the glove sensor. (b) Electronic wiring diagram of the glove sensor. (c) The glove sensor is worn by a user with its coordinate system

$$\begin{bmatrix} g_{adjx} \\ g_{adjy} \\ g_{adjz} \end{bmatrix} = \begin{bmatrix} g_x \\ g_y \\ g_z \end{bmatrix} + \begin{bmatrix} e_x \\ e_y \\ e_z \end{bmatrix} Kp + \begin{bmatrix} \int e_x dt \\ \int e_y dt \\ \int e_z dt \end{bmatrix} Ki \tag{7}$$

Where g_x, g_y, and g_z are angular rates about the x, y, and z axes of the sensor frame measured by 3-axis gyroscope. Equation (8) provides the formula for calculating the quaternion derivative, which describes the rate of change of the Earth frame relative to the sensor frame.

$$\dot{q} = \frac{1}{2} q \otimes \omega_s \tag{8}$$

Where the symbol "⊗" represents the quaternion product, $\omega_s = [0 \quad \omega_x \quad \omega_y \quad \omega_z]$ and $\omega_x = g_{adjx}, \omega_y = g_{adjy}, \omega_z = g_{adjz}$.

$$\dot{q} = \frac{1}{2}\begin{bmatrix} q_0 & -q_1 & -q_2 & -q_3 \\ q_1 & q_0 & -q_3 & q_2 \\ q_2 & q_3 & q_0 & -q_1 \\ q_3 & -q_2 & q_1 & q_0 \end{bmatrix}\begin{bmatrix} 0 \\ \omega_x \\ \omega_y \\ \omega_z \end{bmatrix} \tag{9}$$

The quaternion components (q) can be calculated based on Equation (9) using the numerical integration method. It was implemented in the Simulink block diagram that was embedded in the Arduino Nano microcontroller. The norm (magnitude) of the quaternion q is computed using Equation (10).

$$\begin{bmatrix} q_0 \\ q_1 \\ q_2 \\ q_3 \end{bmatrix} = \frac{1}{norm}\begin{bmatrix} q_0 \\ q_1 \\ q_2 \\ q_3 \end{bmatrix} \tag{10}$$

Finally, the Euler angles can be calculated based on the obtained quaternions as expressed in Equation (11). In this study, only roll and pitch (ϕ, θ) were utilized as the input angles to drive the motion of both left and right extra robotic arms.

$$\begin{bmatrix} \phi \\ \theta \\ \psi \end{bmatrix} = \begin{bmatrix} \text{atan}^2\big(2(q_0q_1 + q_2q_3), 1 - 2(q_1q_1 + q_2q_2)\big) \\ \text{asin}\big(2(q_0q_2 + q_1q_3)\big) \\ \text{atan}^2\big(2(q_0q_3 + q_1q_2), 1 - 2(q_2q_2 + q_3q_3)\big) \end{bmatrix} \tag{11}$$

2.3. Coordinated Motion Control Using Neural Network

Achieving seamless coordination between a biological human arm and ERA is crucial for coordinated motion control. Machine learning offers a powerful solution for this approach. By analyzing a combination of sensor data, such as IMU data (movement and orientation), it can decode the user's intent and then move the extra arm based on the processed signal. This information is then translated into control signals for the robotic arm's servo motors. It can learn complex relationships between user input and desired movements, allowing for natural and coordinated control of the extra limb as if it were an extension of the human body.

The measured yaw angle was not applied because it was prone to drift over time when estimated using the proposed filtering method, which could introduce errors in yaw estimation and make it less reliable for real-time control of the robotic arms as shown in Fig. 13. Additionally, the yaw angle was dependent on the initial yaw angle of the sensor, and variations in its initial conditions can lead to inconsistent calculations, complicating the mapping control input and reducing its effectiveness. By excluding the yaw angle, the study simplifies the control algorithm and ensures more consistent and predictable behavior of the robotic arms. Instead, the focus is on roll and pitch angles, which are more stable, less susceptible to drift, and less affected by initial conditions, enabling more accurate and reliable coordination between the user's hand movements and the ERA.

To train the neural network, input-output data were collected from the attitude angle of the modified glove sensor and corresponding ERA joint angles. Data acquisition involved varying the roll and pitch angles of the ERA through its full range of motion. A total of 75 measurement pairs were recorded for each training dataset. These measurements were grouped into three variations with 25 pairs each: 1) constant 0^0 roll angle with varying pitch, 2) constant 0^0 pitch with varying roll, and 3) varying roll and pitch producing a linear response. This process was performed for both the left and

right ERAs. The roll and pitch inputs from the sensor glove were recorded along with each joint angle Y1, Y2, Y3, and Y4, at each desired position. The collected training data is plotted in Fig. 4 a and Fig. 4 b, showing the input-output mapping for the right and left ERAs, respectively. This dataset forms the basis for training the neural network model to relate the biological user hand movement signals measured by the glove sensor to coordinated multi-joint robotic arm motions through an embodied control interface.

To collect data for mapping human hand movements to the Extra Robotic Arm (ERA) joint angles, a simultaneous recording process was implemented to capture both the hand's roll and pitch angles and the corresponding ERA joint positions. The IMU embedded in the glove sensor measured the user's hand orientation (roll and pitch), while the ERA joint angles were manually recorded for each corresponding hand posture. Data were acquired in three variations to cover different motion ranges: (1) constant roll with varying pitch, (2) constant pitch with varying roll, and (3) simultaneous variation of both roll and pitch. These paired measurements formed the basis for training a neural network model that maps the user's hand movements to the robotic arm's joint angles, enabling coordinated control of the ERA system.

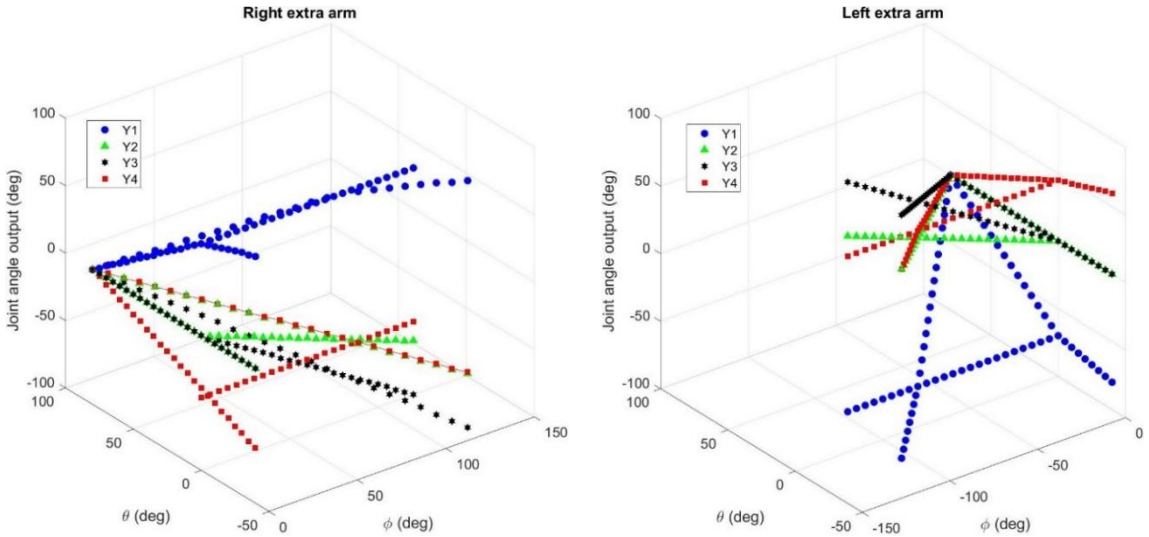

Fig. 4. Data-driven method using neural network regression. (a) Right extra robotic arm, (b) Left extra robotic arm

A total of 75 measurement pairs were collected from a user to construct the neural network training dataset. Each pair represented the angular values for a stable human hand–robot configuration. During each measurement, one operator moved the glove hand to a target posture while another operator manually adjusted the four servo motors of the ERA to achieve the corresponding joint angles. Both the glove and robotic arm were held stationary for approximately 10 seconds to ensure steady readings before proceeding to the next data point. All input and output data were normalized to enhance convergence and computational efficiency. The lightweight neural network was trained without cross-validation, prioritizing simplicity and real-time inference performance for deployment on an embedded microcontroller.

We trained a neural network model with data collected from various postures. This data included measurements of both hand joint angles and each joint angle on the ERA, creating a dataset of paired inputs (human hand posture) and desired outputs (left/right ERA motions). The neural network learned to map these pairings, allowing the system to coordinate the multiple degrees of freedom movements of both the human hand and the ERA.

The proposed coordinated motion feedback control architecture for the extra robotic arms (ERAs) is presented in Fig. 5. The flex sensor on the user's glove detects finger bending motions and wirelessly transmits these signals to the ERA controller, directly driving the soft robotic grippers to perform

grasping actions. Simultaneously, the inertial measurement unit (IMU) on the glove measures the hand's roll and pitch angles, which are sent wirelessly to the main controller. Within the controller, an embedded neural network processes these proprioceptive inputs to compute the corresponding joint angles required for coordinated ERA movements. The controller then actuates each joint through servo motor feedback control, enabling synchronized motion between the user's hand and ERA without relying on external computing systems. Moreover, by maintaining the robotic arm's posture through flex sensor feedback during grasping, the user's biological arms remain free to perform other manipulation tasks. This integrated framework, combining wireless hand sensing and machine learning, achieved embodied proprioceptive coordination between the human and robotic limbs. The overall research methodology flowchart is provided in Supplementary Information Fig. 14.

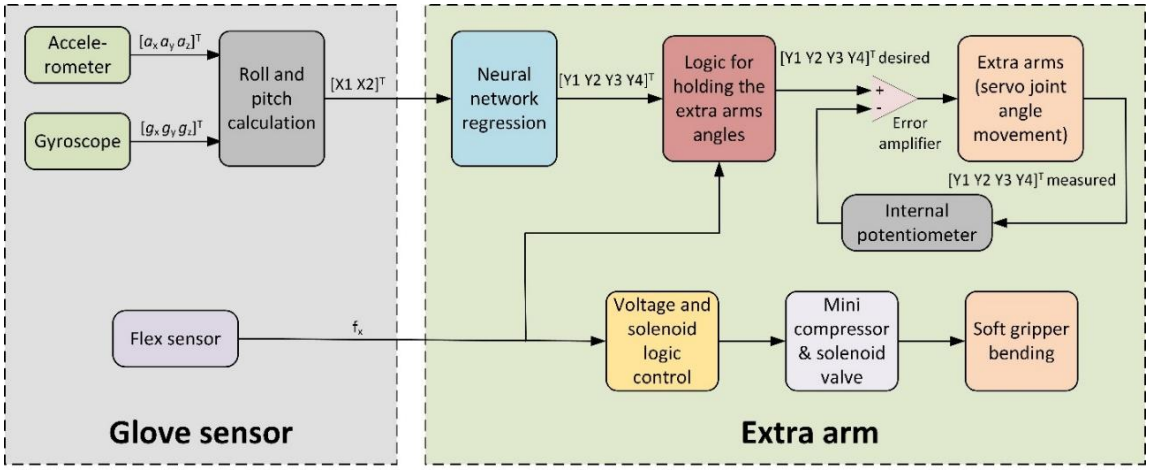

Fig. 5. Control system block diagram for shared coordination control augmented with a soft gripper

3. Results and Discussion

3.1. ERA System Augmented with Soft Robotic Gripper

The ERA system, incorporated with a lightweight 4-DOF arm, achieved dexterous mobility control through servo motor actuation managed by a neural network-based coordination system. To further assess its capabilities, working space simulations were conducted using MATLAB. These simulations demonstrated the ERA's capacity to manipulate objects within a defined working area, with joint angles detailed in Supplementary Information Fig. 15. By generating end-effector trajectories for tasks such as moving objects roughly 200 mm forward, the simulations, along with the resulting end-effector positions, validated the forward kinematics analysis and confirmed the ERA's potential for practical use in the determined working space.

Upon fabricating the soft robotic gripper, bending tests were performed to characterize its pressure-driven actuation capabilities. As shown in Fig. 6 b-c, the soft finger composed of RTV-52 silicone rubber was subjected to variations in both positive and negative pressures. Specifically, Fig. 6 a plots the results of applying pressures ranging from -30 kPa to 30 kPa in 5 kPa increments. The given air pressure (negative pressure) and compression (positive pressure) conditions were explored to characterize the bending motion of the soft finger. The tests revealed that increasing magnitudes of applied pressure (positive or negative) produced greater degrees of bending motion for bending motion. Collectively, the data in Fig. 6 confirmed that the modulated pneumatic actuation could dynamically articulate the soft robotic end-effector through fine control of internal fluidic pressure distributions. This actuation method will be suitable for object-grasping tasks augmented in the ERA.

The soft gripper's bending motion during inflation and deflation is depicted in Fig. 6 b and Fig. 6 c, respectively. Fig. 6 b shows the fingers curving inward under positive pressure for grasping an object. Conversely, Fig. 6 c illustrates the fingers extending outward when negative pressure is applied for object release. This actuation capability is demonstrated in Fig. 6 d, where a drinking bottle is grasped and lifted utilizing positive pressure bending of the soft gripper. For the cooperative control

with the extra robotic arm, user input was mapped to soft finger actuation. As shown in Fig. 6 e and Fig. 6 f, the user could command the closing/flexion of the soft fingers by bending their finger attached to a flex sensor. Meanwhile, the extension of the user's finger resulted in the opening/extension of the soft gripper fingers as depicted in Fig. 6 f. Fig. 6 b-Fig. 6 f validate the soft gripper's capability for grasping and manipulation through pneumatic flexion/extension, as well as its operation as an interface for supernumerary robotic arm assistance directed by natural human finger movements.

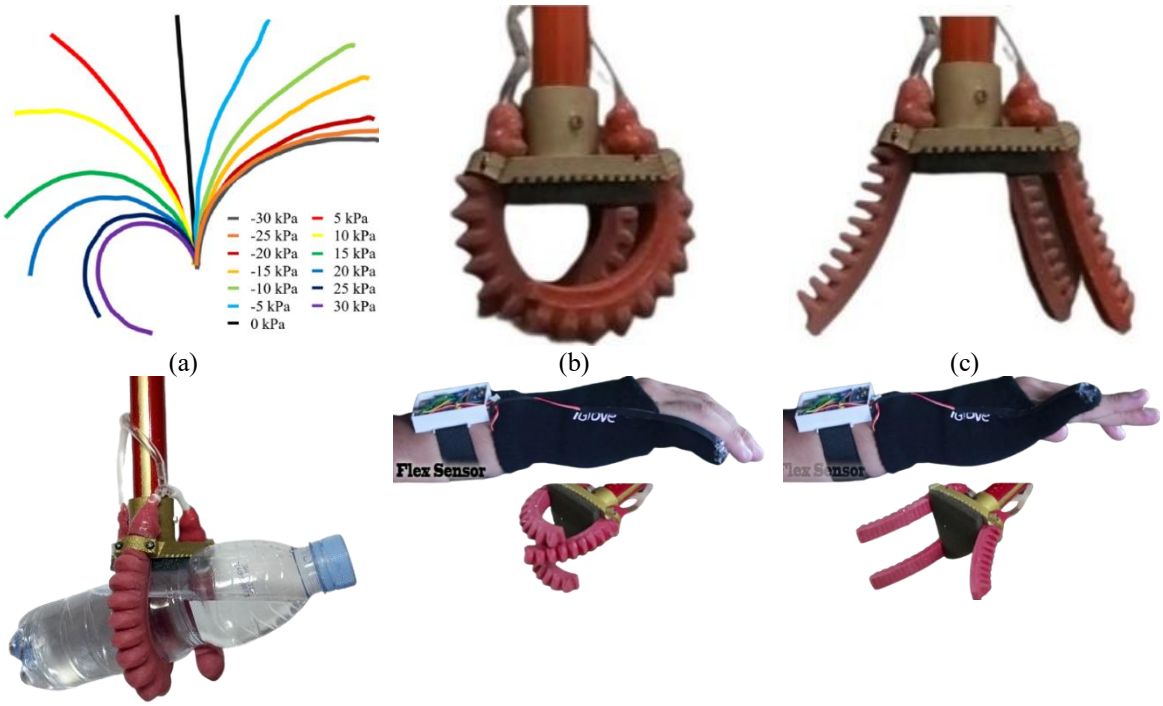

(a) (b) (c)

(d) (500 Grams) (e) (f)

Fig. 6. Grasping control of the soft robotic gripper using the modified sensor glove. (a) Bending motion test, (b) inflation and suction process, (c) deflation and discharge process, (d) maximum weight grasped and lifted, (e) grasping command, and (f) releasing command generated by the flex sensor

The total weight of both ERAs, including the controller, vest, and soft grippers, is 2.8 kg, and each ERA has a total length of 650 mm, ensuring a lightweight and compact design. All components, such as controllers, compressors, valves, and the battery, are integrated into a single wearable vest jacket, minimizing bulk and avoiding the need for external tracking systems by relying on embedded sensors and wireless communication. To ensure minimized energy consumption, a lightweight neural network model was embedded into the microcontroller (Arduino Mega), reducing computational load, and single-precision data processing was employed. The use of miniaturized components (e.g., mini compressors, and solenoid valves) was further selected to minimize the power consumption on the end-effector or soft-robotic gripper.

3.2. Embedded Coordinated Motion with NN Regression

A feedforward neural network architecture was chosen for coordination control between the biological human arm and the extra robotic arm. Due to the Arduino Mega microcontroller's processing and memory constraints, a neural network regression model with five neurons in the input layer was selected to minimize the computational process in the embedded microcontroller. Several hyperparameters were optimized for an effective neural network (NN) regression as summarized in Table 3. The performance error was calculated using mean squared error (MSE) and set to 0.001. MSE can be calculated using Equation (12), which serves as the training performance metric. MSE quantifies the average squared difference between targets and outputs. Lower MSE indicates a better fit to the training data. Validation error was monitored to avoid overfitting. Additionally, the coefficient of the R-value from Equation (13) provided a comparative performance metric independent of dataset scaling.

R-value was calculated to assess how well a regression model fits the data. R compares the actual values (y_i) in the dataset with the estimated values (y'_i) predicted by the model. N is the number of data points. R ranges from 0 to 1, where 0 indicates the worst fit (the model's estimates are far from the actual data) and 1 signifies the best fit (the model's estimates perfectly match the actual data). Minimizing both MSE and maximizing R-value determined the ideal regression architecture for accurately mapping glove sensor inputs to synchronized ERA joint motion outputs, as shown in Fig. 7 a and Fig. 7 b for the right extra arm and Fig. 7 c and Fig. 7 d for the left extra arm. This optimized NN regression model was embedded into the main microcontroller for coordination control of the ERA.

$$MSE = \frac{1}{N}\sum_{i=1}^{N}(y_i - y'_i)^2 \tag{12}$$

$$R = 1 - \frac{\sum_{i=1}^{N}(y_i - y'_i)^2}{\sum_{i=1}^{N} {y_i}^2} \tag{13}$$

Fig. 7 e depicts the generated neural network architecture within a Simulink block diagram, including a single hidden layer with five neurons. This model was selected based on the computational constraints/embedded memory of the target Arduino Mega microcontroller (256 KB of flash memory). To minimize memory usage, all data types were converted from double to single precision, reducing memory size by up to 50% [4]. The "Simulink Support Package for Arduino Hardware" toolbox allowed direct deployment of the trained neural network onto the microcontroller. Four output neurons mapped the glove sensor inputs to coordinated multi-joint extra robotic arm motions. Constrained by the microcontroller's resources, a simple neural network regression model was embedded, resulting in an efficiently structured network that fit within the hardware limitations. The machine learning approach supported coordination control between the human arm and the robotic arm without manual tuning of gain factors or inverse kinematics solutions.

Embedding a neural network on an Arduino MEGA, with its limited 256 KB of flash memory and 8 KB of SRAM, as well as a 16 MHz ATmega2560 microcontroller, requires careful optimization to handle real-time inference efficiently. This study employed a lightweight feedforward neural network with 5 input neurons and 4 output neurons, using single-precision floating-point numbers to reduce memory usage by up to 50% and linear activation functions to minimize computational load. After training, the model was deployed to the Arduino MEGA via the Simulink Support Package for Arduino Hardware, implemented as a Simulink block diagram (Fig. 7 e) that included the neural network architecture and servo motor control logic. Once deployed, the system processed IMU sensor data in real-time, generating joint angle commands for the robotic arms.

Motion-coordinated tests were conducted to validate the real-time coordination between the user's hand movements and the extra robotic arm (ERA). These tests demonstrated the system's capability to mirror the user's hand motions through synchronized ERA movements. The user provided input commands by naturally moving his right hand, and the sensor glove captured the roll (φ) and pitch (θ) orientation or $[x1\ x2]^T$ of the hand. These measured orientation signals were wirelessly transmitted to the ERA controller, where a neural network model mapped the inputs to the corresponding joint angles of the robotic arm $[Y1\ Y2\ Y3\ Y4]^T$. This enabled the ERA to adjust its posture in real-time dynamically, following the user's hand movements without requiring explicit inverse kinematic calculations or manual tuning. The results of these tests are illustrated in Fig. 8, which depicts the real-time coordinated motion between the user's right hand and the right ERA.

Fig. 9 plots the recorded input-output sensorimotor data over measurement periods of 14 seconds for coordinated right-arm motions (Fig. 9 a) and 18 seconds for left-arm motions (Fig. 9 b). By variably moving the user's hands simultaneously, the user dynamically articulated each ERA posture through its range of motion. Based on the test, the neural network regression control enabled the two robotic limbs to follow the user's bimanual gestures without explicit inverse kinematic calculations or

manual tuning. This real-time data-driven method demonstrated the system's potential for natural, embodied assistance through motion coordination enabled by machine learning.

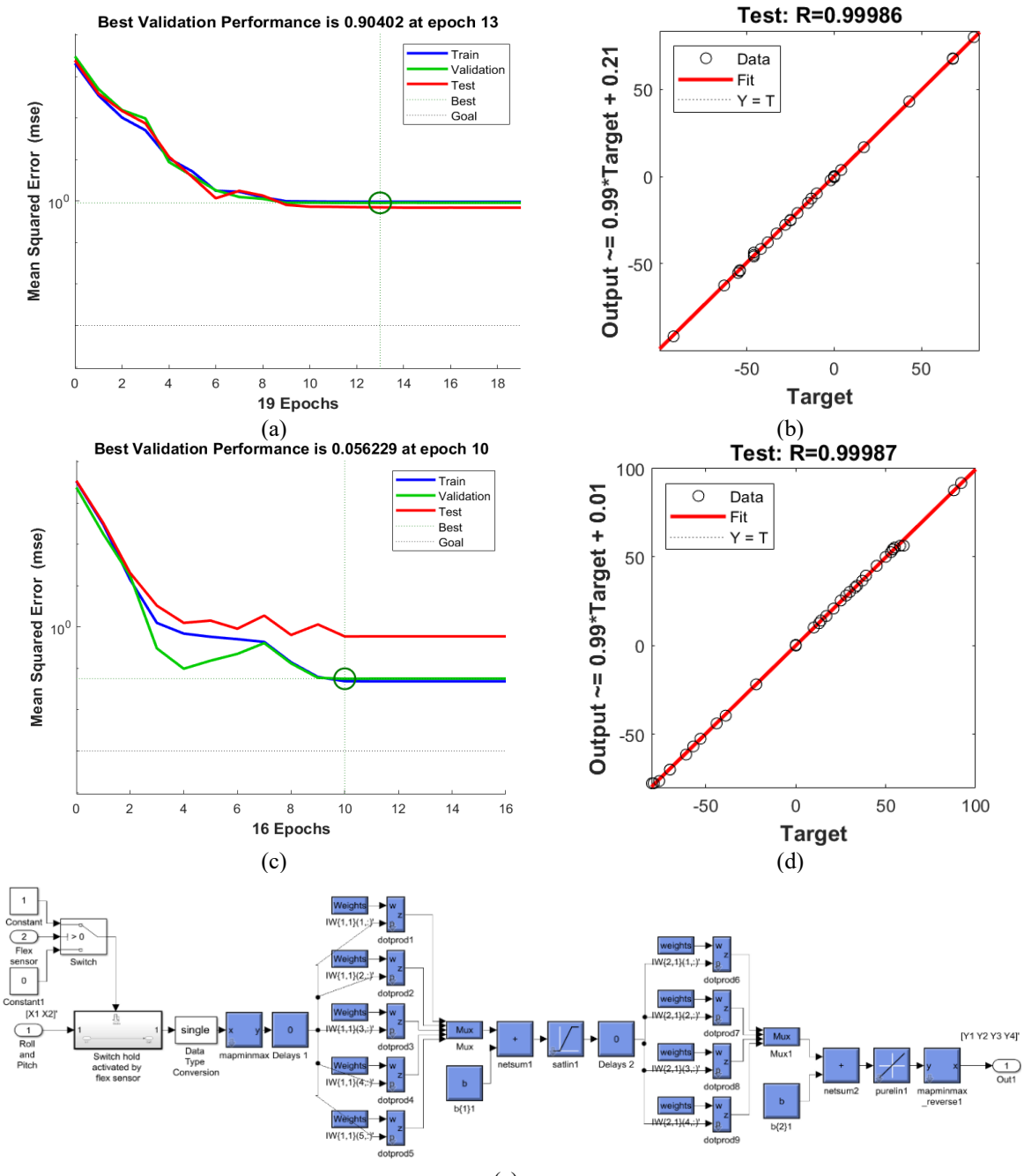

Fig. 7. Neural network regression results. (a) MSE values during training for the right extra arm. (b) R-value during training for the right extra arm. (c) MSE values during training for the left extra arm. (d) R-value during training for the left extra arm. (e) Simulink Block diagram of the embedded neural network regression model. This block diagram was embedded into the Arduino MEGA microcontroller for real-time coordinated motion

Coordinated movement tests assess the integrated system's ability to seamlessly augment with user hand motions for coordinated control of both extra robotic arms. The system leverages a neural network regression for cooperative motion control. Modified glove sensors measuring hand roll and pitch provide natural user inputs. These inputs are mapped in real-time to coordinate multi-joint servo angles, directing the robotic limbs' posture as intended. This functionality aligns with the training dataset presented in Section 2.2.

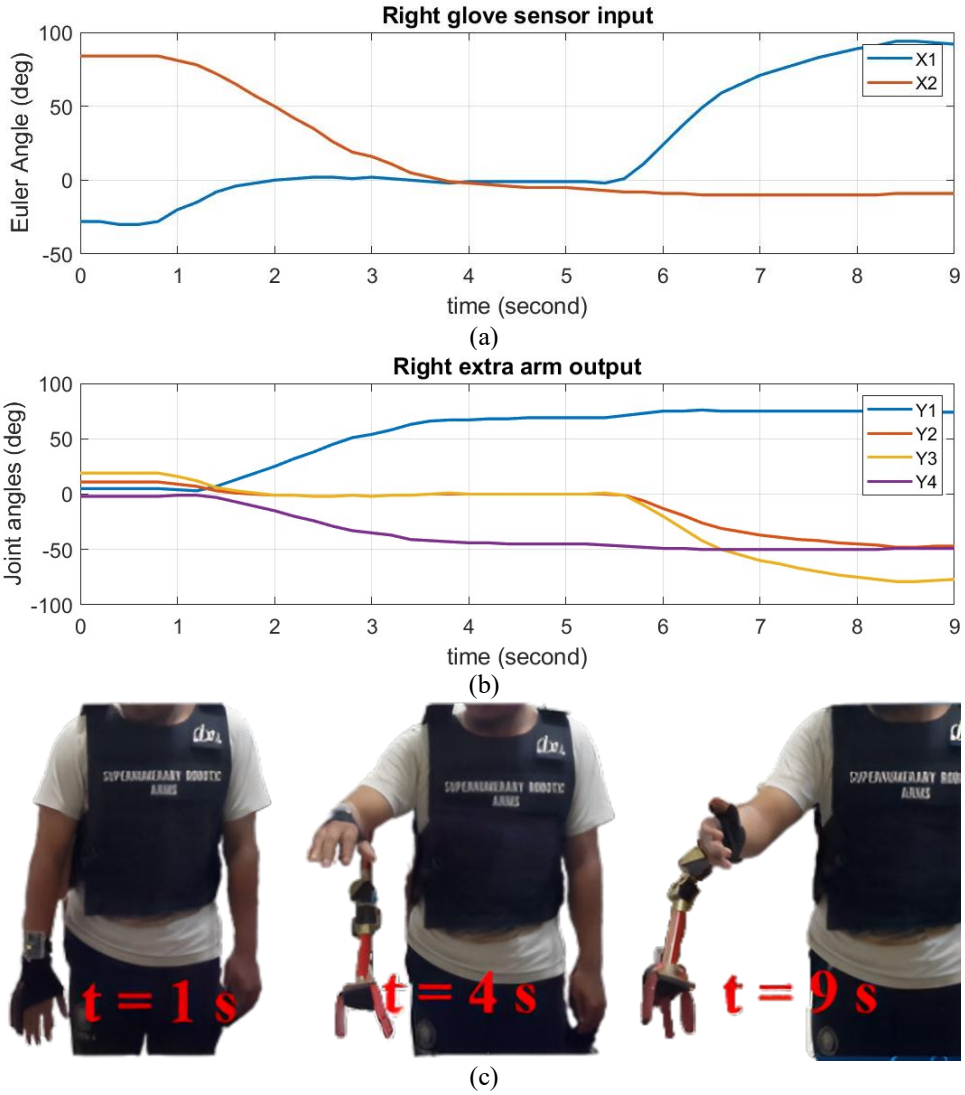

Fig. 8. Real-time coordinated motion between the user's right hand and the right ERA. (a) Orientation input of the human hand movement (roll and pitch). (b) Movement of the four joint angles on the right ERA. (c) Sequential photographs capture the coordinated motion

3.3. Complex Bimanual Manipulation Assistance

After verifying the coordinated movement between human arms and the Extra Robotic Arms (ERAs), the system's ability was evaluated to perform a cooperative object manipulation task. The task involved grasping and transporting multiple objects. The specific task required transferring four cups filled with water from one table to another, as depicted in Fig. 10.

The user began the cooperative object manipulation task by directing both left and right ERAs toward the four plastic cups placed on the table. Simultaneously approaching the cups with the ERAs, the user actuated the integrated soft grippers on each arm by flexing their little fingers to grasp two cups. After achieving a stable bimanual posture with the grasped cups, the user then engaged in a "holding mode" for the ERAs by continuing little finger flexion. This action held the ERAs in place and freed the user's own hands. With his natural arms now available, the user transported the remaining two plastic cups. Upon reaching the destination table, the user relaxed their little fingers to disengage the holding command for the ERAs. Guiding both extra arms, the user then directed them to release the grasped cups onto the new table surface via coordinated release of the soft grippers. Finally, the user placed the last two cups on the table, completing the cooperative multi-object grasping and transport task between his biological arms and augmented ERAs.

The object manipulation task successfully demonstrated the effective cooperation between biological arms and robotic arms in simultaneously transporting multiple objects from one location to another. Specifically, the user's hands and extra robotic arms (ERAs) worked together to grasp four plastic cups, transport them to a new table, and release the cups onto the target surface. This validated that the proposed system involving wearable ERAs augmented with soft grippers can enable fully cooperative manipulation tasks that require precise coordination between biological and ERA.

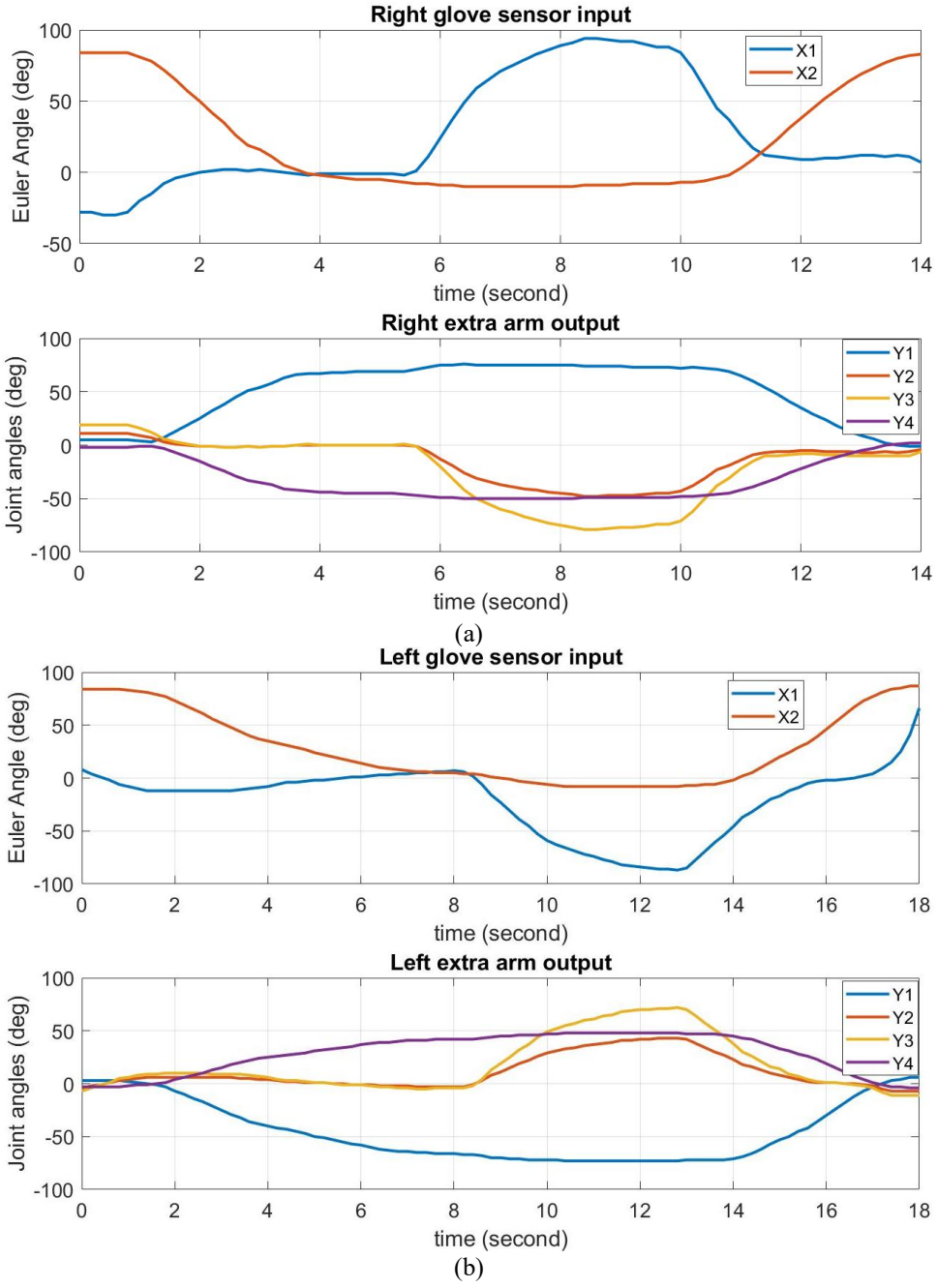

Fig. 9. Input-output measurement test during coordinated motion (a) Right extra arm, (b) Left extra arm

To evaluate the system's ability for complex object manipulation tasks beyond single-person capabilities, seven different tasks were conducted over eight repetitions each with a single user, as summarized in Table 2. These tasks included: 1) transporting and precisely arranging four glasses, 2) opening a doorknob while holding objects, 3) stabilizing a drawing board, 4) steadying a newspaper while performing another task, 5) careful wall-mounting of a large poster, 6) retrieving and hand in item on demand during operating computer, and 7) securely clamping wood for drilling.

Seven cooperative manipulation tasks were conducted, and the results were discussed as Table 2 summarizes key findings. The results of seven tasks can be seen in Supplementary Video S2 (https://bit.ly/3Td3fFb). Transporting multiple glasses simultaneously, as mentioned before (Task 1) achieved 100% success, demonstrating that extra arms are highly effective for the cooperative carrying of items. The soft gripper could grasp and hold objects firmly weighing less than 500 grams. Tasks requiring coordinated manipulation across both human and robotic arms, such as door opening (Task 2) and page-turning (Task 4), showed success rates of 75-87.5% respectively, suggesting refinement is still needed to improve the synchronization and replace the soft gripper with more rigid ones, such as a robotic hand. Support roles like stabilizing boards for drawing/drilling (Tasks 3, 7) achieved full 100% success, confirming that extra arms excel at steady holding without complex motion. The gripper could hold the objects firmly, and the user could use his arms when the extra arm posture was held. Precisely placing a large poster cooperatively with the extra arms (Task 5) resulted in the lowest success rate of 50%, suggesting that multi-arm coordination remained challenging. This limitation might stem from potential shortcomings in motion synchronization, control latency, and spatial awareness, which together hindered the precise alignment between the arms and the poster. Additionally, the soft gripper's limited ability to securely/firmly grasp the thin poster further contributed to the reduced performance.

Fig. 10. Cooperative object manipulation task between biological arms and extra arms

Table 2. Coordination control tasks for challenging object manipulation. The videos for object multi-arm cooperation manipulation tasks can be seen in Supplementary Video S2 (https://bit.ly/3Td3fFb)

No	Object manipulation assisted with extra arms	Photo	Number of trials	Success trial	Success trial
1.	Extra robotic arms assisted human arms to pick up, carry, and place four glasses on the table.		8	8	100%
2.	While the user grasped an object in each hand, the extra arms assisted by opening the doorknob.		8	7	87.5%
3.	With the help of robotic arms holding the drawing board, allowing the user to draw freely.		8	8	100%
4.	Extra arms hold the newspaper board steady, allowing the user to sip coffee with one hand and turn pages with the other.		8	6	75%
5.	In a coordinated effort, the user's arms worked alongside two robotic arms to precisely place an A2 poster on the wall.		8	4	50%
6.	While operating a computer, the user reached for a bottle of water with a robotic arm and handed it to someone.		8	8	100%
7.	The user wielded a hand drill while robotic arms securely clamped the wood in place for precise drilling.		8	8	100%

The seven cooperative manipulation tasks were performed by a single user whose data were not included during the neural network training stage. Despite the user being excluded from the training

dataset, the embedded lightweight neural network, operating entirely within the constrained microcontroller, successfully translated the user's real-time hand posture into coordinated movements of both ERAs. The user executed all seven tasks, including multi-object transport, door operation, stabilization, and tool-assisted manipulation, demonstrating that the neural network model effectively generalized to a new user without requiring additional calibration. These findings confirm the scalability and robustness of the embedded proprioceptive mapping approach, validating that the wearable ERA system can naturally assist a user in performing complex multi-arm cooperative tasks even when the user was not part of the model training phase.

3.4. Discussion ERA Augmented with Soft Gripper

Integrating soft robotic grippers with the Extra Robotic Arms (ERA) system facilitated adaptive and gentle object manipulation, successfully handling varied shapes and weights like glasses and wood through compliant pneumatic actuation; however, limitations arose with smooth or thin objects due to insufficient frictional grip. While the lightweight design and wireless sensor glove control enhanced usability and demonstrated human-robot collaboration via neural network mapping, future improvements should focus on hybrid gripper designs and refined control algorithms to enhance precision, particularly for complex bimanual tasks.

3.5. Real-Time Coordinated Motion

The proposed system enabled real-time control of two ERAs by translating human hand posture and intention captured by a wearable glove. This glove integrates flex sensors to capture finger bending and an IMU to measure hand orientation, wirelessly transmitting this data via a 2.4 GHz module to the ERA controller. An embedded neural network directly maps the incoming sensor data, specifically the roll and pitch angles representing hand motion/intention, to the corresponding joint angles of the robotic arms. Once these commands are generated, the servos are actuated immediately, establishing a continuous loop that ensures smooth, real-time motion mirroring without perceptible delay, effectively allowing the user to control the ERAs as natural, responsive extensions of the user's own body. The SRL's reliance on interpreting human intent is fundamental for achieving seamless human–robot collaboration (HRC), a critical area of research with applications in wearable robots and collaborative arms [58]-[62]. Previous work has focused on improving predictive dynamics in HRC using a combination of height sensors and adaptive Kalman filtering [63], while others have used Linear Discriminant Analysis (LDA) to estimate joint degrees of freedom from limb movements [64]. Similarly, systems using surface electromyography (sEMG) signals have been developed to detect human gestures and intuitively guide robotic exoskeletons using an adaptive neural network controller [65]. The proposed ERA system was developed on these foundations by deploying an embedded neural network for direct, real-time mapping from hand posture to robotic arm commands, simplifying the control pipeline.

The efficacy of the real-time operation and coordination control was tested through coordinated movement tests and object manipulation tasks. Based on the test results, the direct mapping from the user's hand movements to the ERA's joint angles allowed the robotic arms to perform practical tasks, such as grasping and lifting objects, in sync with the user's natural motions. A key advantage demonstrated was that the neural network-based control system enabled the ERA to follow the user's hand posture without the computational burden of explicit inverse kinematics calculations or the need for manual tuning. This real-time responsiveness proved critical during cooperative object manipulation tasks, like transporting cups or opening a doorknob, where the ERA responded instantly to the user's input. The ERA system maintained a low delay (less than 0.5 seconds), which is essential for high-precision tasks such as holding a drawing board steady or grasping and lifting four objects simultaneously, proving its capability for responsive cooperation.

3.6. Complex Bimanual Manipulation Assistance

The experimental results demonstrated that the proposed ERA system was capable of successfully executing seven distinct complex bimanual manipulation tasks. These tasks, ranging from

multiple object placement to complex tool handling, are inherently challenging for an individual with two arms. The demonstrated capabilities, including picking up and placing multiple objects, opening doors while encumbered, facilitating drawing, managing reading materials while consuming beverages, poster placement, multiple object transfer, and tool-assisted drilling, indicate that the ERA is particularly well-suited for users in healthy conditions who require assistance with such complex manipulations.

Among the tested tasks, several demonstrated how the ERA can support both practical and situational human activities in daily life. Task 1, involving the transportation of multiple items, showed the system's capability to assist users in managing several objects simultaneously. Task 2, opening a door while holding objects, illustrated its usefulness in maintaining mobility and independence when the user's hands are occupied. Task 3, facilitating drawing, highlighted the potential for creative or precision-based activities. Task 4, managing reading materials while consuming beverages, demonstrated its convenience in multitasking and leisure contexts. Task 5, precise poster placement, showcased its assistance in tasks requiring accuracy and stability. Task 6, reaching for and transferring items while engaged in desk work, emphasized its ability to enhance accessibility and comfort in work environments. Finally, task 7, utilizing tools with precision and assistance, illustrated how the ERA can augment dexterity and coordination for tasks requiring dual-handed operation. Together, these tasks collectively demonstrate the system's versatility in supporting diverse human-robot cooperation.

The proposed study demonstrates a shared coordinated motion control in wearable robotics by embedding a lightweight neural network directly onto a low-power microcontroller, enabling real-time proprioceptive mapping and coordinated control of dual 4-DOF ERA equipped with soft grippers. The system's seamless integration of hardware and software achieved natural cooperation between human and robotic motion, validated through seven multi-arm manipulation tasks that confirmed its practicality and computational efficiency. However, the work remains preliminary, with evaluations limited to a small number of participants, task variations, and ergonomics results. The system's adaptability across diverse users, handling of thin or slippery objects due to gripper compliance, absence of tactile feedback, and occasional coordination latency highlight areas for improvement in robustness, precision, and general usability in future study.

4. Conclusion

This study successfully demonstrated the feasibility of an embedded, data-driven control approach for wearable extra robotic arms integrated with soft grippers and a sensor glove interface. By embedding a lightweight neural network directly into a constrained microcontroller, real-time proprioceptive mapping between the user's biological hand posture and the robotic limbs was achieved without an external computation or inverse kinematic modeling. Seven human-robot cooperation tasks confirmed that this embedded neural network could efficiently process sensory inputs and generate coordinated servo responses in real time, enabling seamless cooperation between human and robotic arms. The results from seven cooperative manipulation tasks showed that the system can effectively assist users in performing complex multi-arm operations, such as object transport, stabilization, and tool handling, that would otherwise be difficult for a single person. These findings demonstrate that embedding a data-driven model on low-power hardware is both computationally feasible and practical for achieving natural, low-latency shared control in wearable robotics. This study was limited to a single user, not included in the training data, and its seven manipulation tasks lacked specific performance metrics. To build upon this foundation, future work will focus on expanded user studies with diverse participants to quantitatively evaluate usability and adaptation. In parallel, the technical enhancements, such as integrating a hybrid rigid-soft gripper with advanced learning algorithms, will be explored to improve the system's grasp stability, adaptability, and robustness.

Supplementary Materials: The study data of this work can be shared upon request.

Author contribution: MM: Conceptualization, Methodology, Writing – review & editing. MA: Supervision, Writing – review & editing, Software. JDS: Supervision, Methodology. DM: data acquisition, experiments, Hardware, TN: data acquisition, experiments, Hardware.

Funding: This research was partially supported by Diponegoro University through the International Scientific Publication under contract No. 569-133/UN7.D2/PP/V/2023.

Acknowledgements: The authors would like to acknowledge Diponegoro University for their support of this research work.

Conflicts of Interest: The authors declare that they have no competing interests.

Appendix

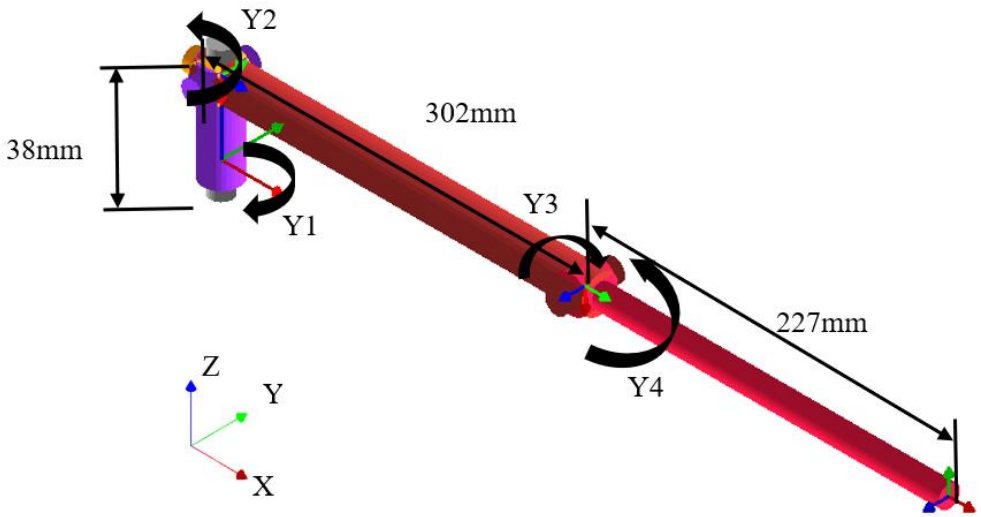

Fig. 11. Four DOF extra robotic arms with four revolute joints in the XYZ cartesian coordinate. Each joint input/NN regression command input [Y1, Y2, Y3, Y4] on the revolute joints corresponds with its joint angle input in Equation (2). Where Y1 = θ_1, Y2 = θ_2, Y3 = θ_3, and Y1 = θ_4. In equation (2), X, Y, and Z refer to the end-effector position in the XYZ coordinate system

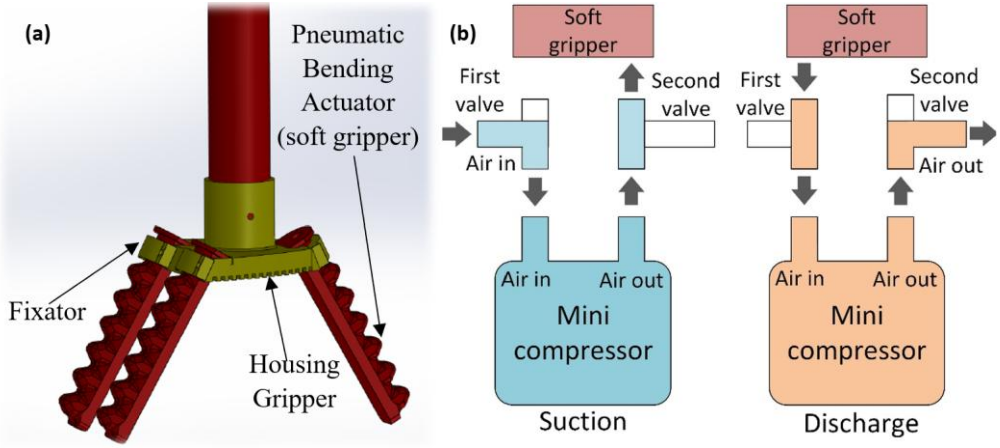

Fig. 12. Three-fingered soft robotic gripper. (a) Design of the soft gripper that can be attached to the end of each ERA, (b) Mechanism design for controlling the bending motion of the gripper. The soft robotic gripper applied a mini air compressor and two solenoid valves to control its finger-bending motion. Inflating the fingers involves closing one valve and opening another, allowing pressurized air to bend the fingers. Deflating the fingers works in reverse, trapping air inside and using the compressor to suck it out, causing the fingers to straighten. This system allows precise open-loop control of the gripper for grasping and releasing objects

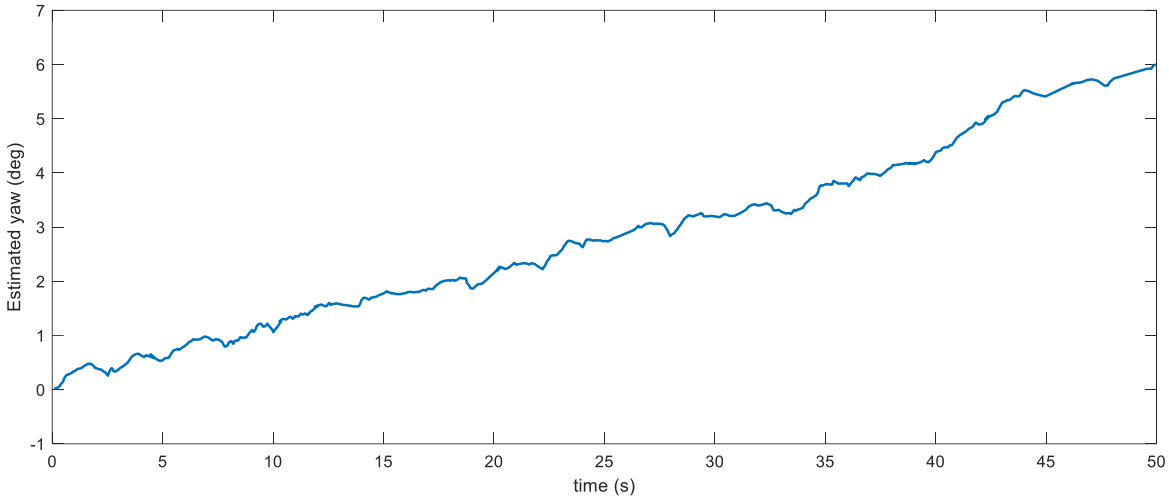

Fig. 13. Measured yaw angle obtained from the filter, showing the presence of drift error

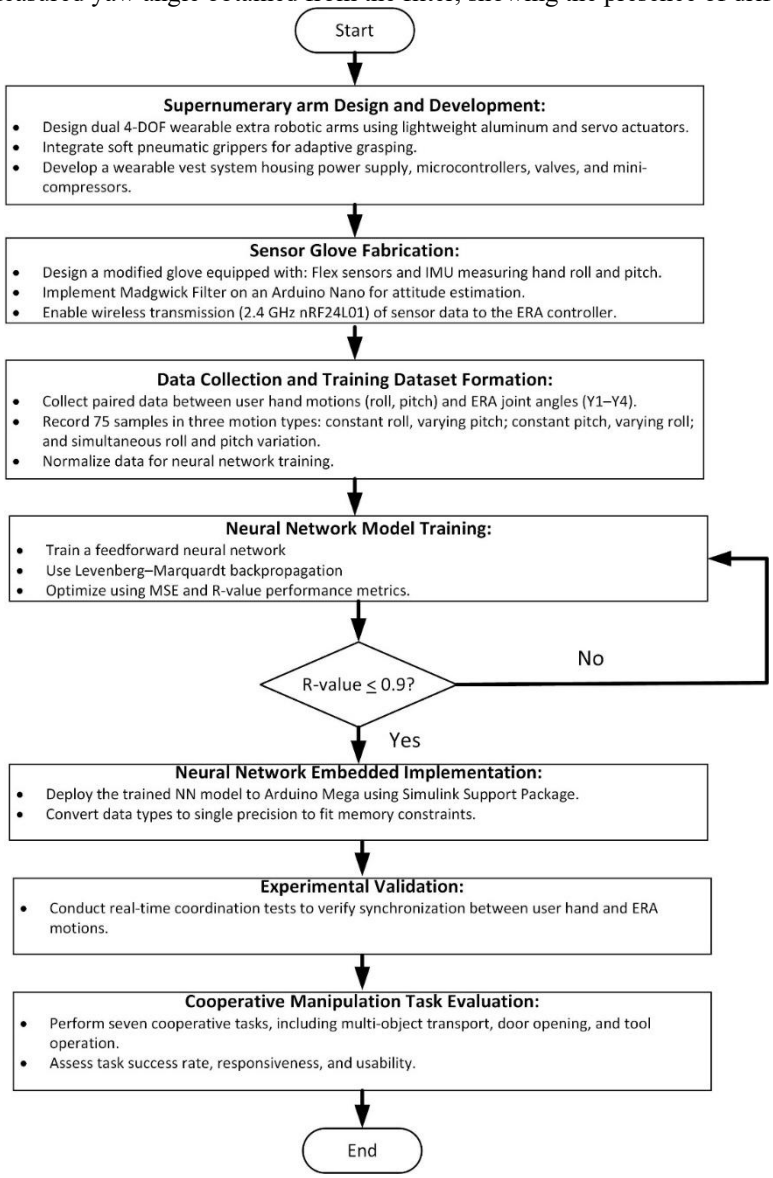

Fig. 14. Overall research method flowchart. This diagram illustrates the sequential stages of the project, including supernumerary arm design, sensor glove fabrication, data collection, neural network training and deployment, experimental validation, and cooperative task evaluation

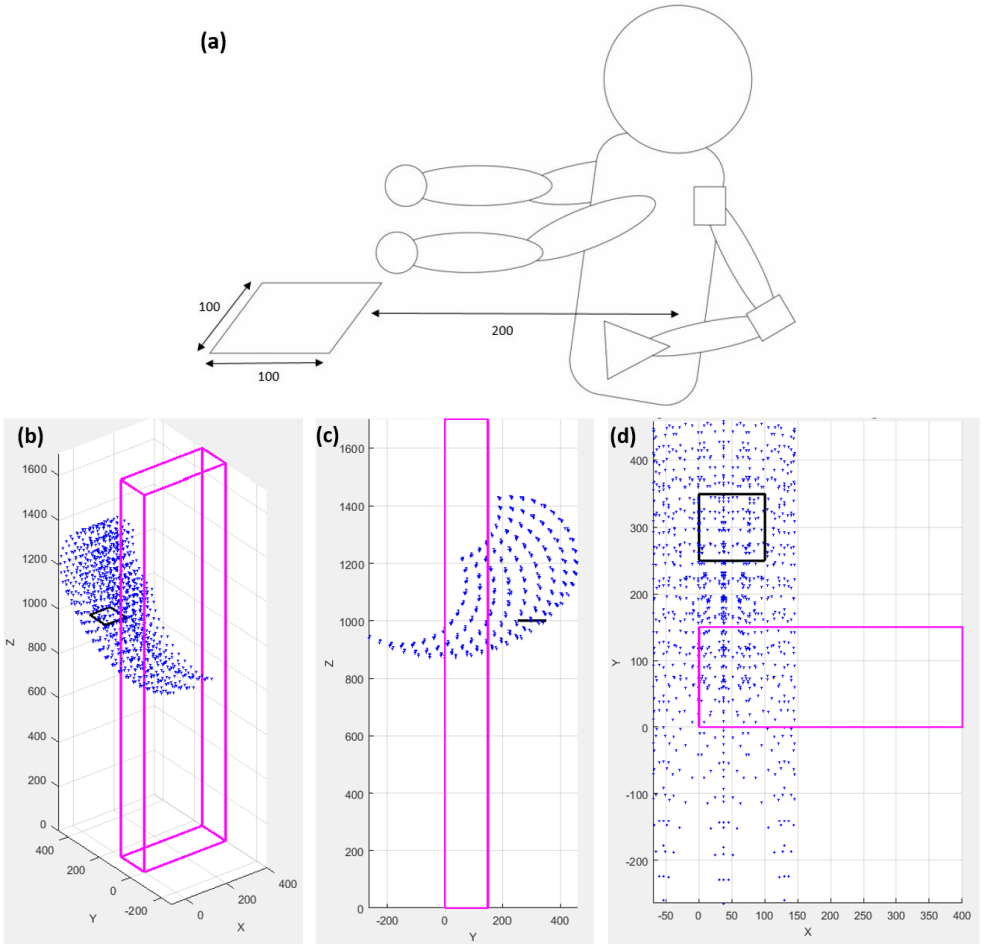

Fig. 15. ERA Working Space Simulation. (a) Illustration of the working scenario. Working space simulation results are shown for (b) the 3-axis X-Y-Z, (c) the X-Z plane, and (d) the X-Y plane. In this scenario, to transport an object, the worker picked up the object and placed it at the desired position, approximately 200 mm in front. The object, with dimensions of 100 mm in length and 100 mm in width, was selected as the working object. For the simulation, joint angles were input into the forward kinematics equations. MATLAB software generated the end-effector points and displayed the trajectory graph. The joint angle inputs used for the simulation are as follows: Y1 = -30:10:50, Y2 = 80:10:100, Y3 = 80:10:100, and Y4 = 50:10:90. The simulation results illustrate the working space of the proposed ERA

Table 3. Hyperparameter selection for the SRA's embedded neural network

Parameter	Value
Model	Feed-forward neural network
Number of neurons (Hidden Layer)	5
Divide Parameter	Random
Ratio of Training	70%
Ratio of Validation	15%
Ratio of Testing	15%
Training Algorithm	Levenberg-Marquardt backpropagation
Maximum Epoch	1000
Performance Goal	0.001
Error Performance	Mean Squared Error (MSE)
Transfer function of Layer 1 (Hidden Layer)	Saturating linear transfer function (satlin)
Transfer function of Layer 2 (Output Layer)	Linear transfer function (purelin)

Supplementary Videos

Video S1. This wearable robotic system consists of a pair of four-degree-of-freedom (4-DOF) extra arms, each equipped with a three-fingered soft gripper. The system's core components are two main

controllers, a battery, mini compressors, and a wireless module that are housed in a backpack worn by the user. A specialized vest supports the backpack. Coordinated control of the extra arms and soft grippers is achieved through a modified glove incorporating an IMU, stretch sensor, microcontroller, and wireless communication.

Video S1 link: https://bit.ly/43Zz36I.

Various Cooperative Object Manipulation Tasks

Video S2. To assess the system's capabilities for complex, collaborative tasks, a single user performed seven different tasks, repeated eight times for each task. These tasks are summarized below:

- Precisely reaching, grasping, transporting, and arranging four glasses.
- Opening a doorknob while holding objects.
- Stabilizing a drawing board when the human hand is drawing on the board.
- Steadying a newspaper during another task.
- Carefully wall-mounting a large poster.
- Retrieving and handing over items on demand while using a computer.
- Securely clamp wood for drilling.

Video S2 Link: https://bit.ly/3Td3fFb.

References

[1] N. Segura Meraz, M. Sobajima, T. Aoyama, and Y. Hasegawa, “Modification of body schema by use of extra robotic thumb,” *ROBOMECH Journal*, vol. 5, no. 1, p. 3, 2018, https://doi.org/10.1186/s40648-018-0100-3.

[2] A. Shafti, S. Haar, R. Mio, P. Guilleminot, and A. A. Faisal, “Playing the piano with a robotic third thumb: assessing constraints of human augmentation,” *Scientific Reports*, vol. 11, no. 1, p. 21375, 2021, https://doi.org/10.1038/s41598-021-00376-6.

[3] I. Hussain *et al*., “A soft supernumerary robotic finger and mobile arm support for grasping compensation and hemiparetic upper limb rehabilitation,” *Robotics and Autonomous Systems*, vol. 93, pp. 1-12, 2017, https://doi.org/10.1016/j.robot.2017.03.015.

[4] J. D. Setiawan, M. Ariyanto, M. Munadi, M. Mutoha, A. Glowacz, and W. Caesarendra, “Grasp Posture Control of Wearable Extra Robotic Fingers with Flex Sensors Based on Neural Network,” *Electronics*, vol. 9, no. 6, p. 905, 2020, https://doi.org/10.3390/electronics9060905.

[5] F. Y. Wu and H. H. Asada, "Implicit and Intuitive Grasp Posture Control for Wearable Robotic Fingers: A Data-Driven Method Using Partial Least Squares," *IEEE Transactions on Robotics*, vol. 32, no. 1, pp. 176-186, 2016, https://doi.org/10.1109/TRO.2015.2506731.

[6] F. Y. Wu and H. H. Asada, "“Hold-and-manipulate” with a single hand being assisted by wearable extra fingers," *2015 IEEE International Conference on Robotics and Automation (ICRA)*, pp. 6205-6212, 2015, https://doi.org/10.1109/ICRA.2015.7140070.

[7] Q. Zhang *et al*., “Motion-Compensation Control of Supernumerary Robotic Arms Subject to Human-Induced Disturbances,” *Advanced Intelligent Systems*, vol. 6, no. 5, p. 2300448, 2024, https://doi.org/10.1002/aisy.202300448.

[8] P. H. Daniel, C. Fu and H. H. Asada, "Musculoskeletal Load Analysis for the Design and Control of a Wearable Robot Bracing the Human Body While Crawling on a Floor," *IEEE Access*, vol. 10, pp. 6814-6829, 2022, https://doi.org/10.1109/ACCESS.2021.3134056.

[9] M. Kusunoki, L. V. Nguyen, H. -R. Tsai, V. A. Ho and H. Xie, "Scalable and Foldable Origami-Inspired Supernumerary Robotic Limbs for Daily Tasks," *IEEE Access*, vol. 12, pp. 53436-53447, 2024, https://doi.org/10.1109/ACCESS.2024.3387485.

[10] B. Llorens - Bonilla, F. Parietti and H. H. Asada, "Demonstration-based control of supernumerary robotic limbs," *2012 IEEE/RSJ International Conference on Intelligent Robots and Systems*, pp. 3936-3942, 2012, https://doi.org/10.1109/IROS.2012.6386055.

[11] J. Luo *et al*., "Modeling and Balance Control of Supernumerary Robotic Limb for Overhead Tasks," *IEEE Robotics and Automation Letters*, vol. 6, no. 2, pp. 4125-4132, 2021, https://doi.org/10.1109/LRA.2021.3067850.

[12] G. Dominijanni *et al*., "The neural resource allocation problem when enhancing human bodies with extra robotic limbs," *Nature Machine Intelligence*, vol. 3, no. 10, pp. 850-860, 2021, https://doi.org/10.1038/s42256-021-00398-9.

[13] V. Vatsal and G. Hoffman, "The Wearable Robotic Forearm: Design and Predictive Control of a Collaborative Supernumerary Robot," *Robotics*, vol. 10, no. 3, p. 91, 2021, https://doi.org/10.3390/robotics10030091.

[14] F. Parietti, K. C. Chan, B. Hunter and H. H. Asada, "Design and control of Supernumerary Robotic Limbs for balance augmentation," *2015 IEEE International Conference on Robotics and Automation (ICRA)*, pp. 5010-5017, 2015, https://doi.org/10.1109/ICRA.2015.7139896.

[15] L. Treers *et al*., "Design and Control of Lightweight Supernumerary Robotic Limbs for Sitting/Standing Assistance," *2016 International Symposium on Experimental Robotics*, pp. 299-308, 2017, https://doi.org/10.1007/978-3-319-50115-4_27.

[16] F. Parietti and H. Asada, "Supernumerary Robotic Limbs for Human Body Support," *IEEE Transactions on Robotics*, vol. 32, no. 2, pp. 301-311, 2016, https://doi.org/10.1109/TRO.2016.2520486.

[17] M. Hao, J. Zhang, K. Chen, H. Asada, and C. Fu, "Supernumerary Robotic Limbs to Assist Human Walking With Load Carriage," *Journal of Mechanisms and Robotics*, vol. 12, no. 6, p. 061014, 2020, https://doi.org/10.1115/1.4047729.

[18] C. Khazoom, P. Caillouette, A. Girard and J. -S. Plante, "A Supernumerary Robotic Leg Powered by Magnetorheological Actuators to Assist Human Locomotion," *IEEE Robotics and Automation Letters*, vol. 5, no. 4, pp. 5143-5150, 2020, https://doi.org/10.1109/LRA.2020.3005629.

[19] D. J. Gonzalez and H. H. Asada, "Design of Extra Robotic Legs for Augmenting Human Payload Capabilities by Exploiting Singularity and Torque Redistribution," *2018 IEEE/RSJ International Conference on Intelligent Robots and Systems (IROS)*, pp. 4348-4354, 2018, https://doi.org/10.1109/IROS.2018.8593506.

[20] J. Nie, Y. Sugahara and Y. Takeda, "Design of Wearable Robotic Support Limbs for Walking Assistance Based on Configurable Support Polygon," *2022 IEEE 3rd International Conference on Human-Machine Systems (ICHMS)*, pp. 1-6, 2022, https://doi.org/10.1109/ICHMS56717.2022.9980804.

[21] N. Alam, S. Hasan, G. A. Mashud, and S. Bhujel, "Neural Network for Enhancing Robot-Assisted Rehabilitation: A Systematic Review," *Actuators*, vol. 14, no. 1, p. 16, 2025, https://doi.org/10.3390/act14010016.

[22] A. Mohebbi, "Human-Robot Interaction in Rehabilitation and Assistance: a Review," *Current Robotics Reports*, vol. 1, no. 3, pp. 131-144, 2020, https://doi.org/10.1007/s43154-020-00015-4.

[23] X. Zhang, Y. Qu, G. Zhang, Z. Wang, C. Chen, and X. Xu, "Review of sEMG for Exoskeleton Robots: Motion Intention Recognition Techniques and Applications," *Sensors*, vol. 25, no. 8, p. 2448, 2025, https://doi.org/10.3390/s25082448.

[24] H. Hayashi and T. Tsuji, "Human–Machine Interfaces Based on Bioelectric Signals: A Narrative Review with a Novel System Proposal," *IEEJ Transactions on Electrical and Electronic Engineering*, vol. 17, no. 11, pp. 1536-1544, 2022, https://doi.org/10.1002/tee.23646.

[25] B. Brahmi, M. Saad, A. Brahmi, C. O. Luna, and M. H. Rahman, "Compliant control for wearable exoskeleton robot based on human inverse kinematics," *International Journal of Advanced Robotic Systems*, vol. 15, no. 6, p. 1729881418812133, 2018, https://doi.org/10.1177/1729881418812133.

[26] D. Bedolla-Martinez, Y. Kali, M. Saad, C. Ochoa-Luna, and M. H. Rahman, "Learning human inverse kinematics solutions for redundant robotic upper-limb rehabilitation," *Engineering Applications of Artificial Intelligence*, vol. 126, p. 106966, 2023, https://doi.org/10.1016/j.engappai.2023.106966.

[27] Y. Ning, L. Sang, H. Wang, Q. Wang, L. Vladareanu, and J. Niu, "Upper limb exoskeleton rehabilitation robot inverse kinematics modeling and solution method based on multi-objective optimization," *Scientific Reports*, vol. 14, no. 1, p. 25476, 2024, https://doi.org/10.1038/s41598-024-77137-8.

[28] Y. M. Zhou, C. Hohimer, T. Proietti, C. T. O'Neill and C. J. Walsh, "Kinematics-Based Control of an Inflatable Soft Wearable Robot for Assisting the Shoulder of Industrial Workers," *IEEE Robotics and Automation Letters*, vol. 6, no. 2, pp. 2155-2162, 2021, https://doi.org/10.1109/LRA.2021.3061365.

[29] J. Wang, L. Bi and W. Fei, "EEG-Based Motor BCIs for Upper Limb Movement: Current Techniques and Future Insights," *IEEE Transactions on Neural Systems and Rehabilitation Engineering*, vol. 31, pp. 4413-4427, 2023, https://doi.org/10.1109/TNSRE.2023.3330500.

[30] H.-B. Li, Z. Li, L. He, and X.-R. Guan, "Wearable Extra Robotic Limbs: A Systematic Review of Current Progress and Future Prospects," *Journal of Intelligent & Robotic Systems*, vol. 109, no. 1, p. 16, 2023, https://doi.org/10.1007/s10846-023-01940-0.

[31] G. Salvietti *et al*., "Integration of a Passive Exoskeleton and a Robotic Supernumerary Finger for Grasping Compensation in Chronic Stroke Patients: The SoftPro Wearable System," *Frontiers in Robotics and AI*, vol. 8, 2021, https://doi.org/10.3389/frobt.2021.661354.

[32] H. Alsuradi, J. Hong, H. Mazi, and M. Eid, "Neuro-motor controlled wearable augmentations: current research and emerging trends," *Frontiers in Neurorobotics*, vol. 18, 2024, https://doi.org/10.3389/fnbot.2024.1443010.

[33] Y. Tong and J. Liu, "Review of Research and Development of Supernumerary Robotic Limbs," *IEEE/CAA Journal of Automatica Sinica*, vol. 8, no. 5, pp. 929-952, 2021, https://doi.org/10.1109/JAS.2021.1003961.

[34] D. Prattichizzo *et al*., "Human augmentation by wearable supernumerary robotic limbs: review and perspectives," *Progress in Biomedical Engineering*, vol. 3, no. 4, p. 042005, 2021, https://doi.org/10.1088/2516-1091/ac2294.

[35] B. Yang, J. Huang, X. Chen, C. Xiong and Y. Hasegawa, "Supernumerary Robotic Limbs: A Review and Future Outlook," *IEEE Transactions on Medical Robotics and Bionics*, vol. 3, no. 3, pp. 623-639, 2021, https://doi.org/10.1109/TMRB.2021.3086016.

[36] Y. Liu, Z. Wang, S. Huang, W. Wang, and D. Ming, "EEG characteristic investigation of the sixth-finger motor imagery and optimal channel selection for classification," *Journal of Neural Engineering*, vol. 19, no. 1, p. 016001, 2022, https://doi.org/10.1088/1741-2552/ac49a6.

[37] C. Penaloza, D. Hernandez-Carmona and S. Nishio, "Towards Intelligent Brain-Controlled Body Augmentation Robotic Limbs," *2018 IEEE International Conference on Systems, Man, and Cybernetics (SMC)*, pp. 1011-1015, 2018, https://doi.org/10.1109/SMC.2018.00180.

[38] Z. Tang, H. Wang, Z. Cui, J. Ding, and L. Zhang, "Design of a Supernumerary Robotic Limb Based on Hybrid Control of Motion Imagination and Object Detection," *Design Studies and Intelligence Engineering*, pp. 88-96, 2024, https://doi.org/10.3233/FAIA231428.

[39] M. Y. Saraiji, T. Sasaki, K. Kunze, K. Minamizawa, and M. Inami, "MetaArms: Body Remapping Using Feet-Controlled Artificial Arms," *Proceedings of the 31st Annual ACM Symposium on User Interface Software and Technology (UIST '18)*, pp. 65-74, 2018, https://doi.org/10.1145/3242587.3242665.

[40] M. Ariyanto, M. Munadi, J. D. Setiawan, D. Mulyanto and T. Nugroho, "Three-Fingered Soft Robotic Gripper Based on Pneumatic Network Actuator," *2019 6th International Conference on Information Technology, Computer and Electrical Engineering (ICITACEE)*, pp. 1-5, 2019, https://doi.org/10.1109/ICITACEE.2019.8904145.

[41] Y. Ye, P. Cheng, B. Yan, Y. Lu, and C. Wu, "Design of a Novel Soft Pneumatic Gripper with Variable Gripping Size and Mode," *Journal of Intelligent & Robotic Systems*, vol. 106, no. 1, p. 5, 2022, https://doi.org/10.1007/s10846-022-01721-1.

[42] W. Park, S. Seo and J. Bae, "A Hybrid Gripper With Soft Material and Rigid Structures," *IEEE Robotics and Automation Letters*, vol. 4, no. 1, pp. 65-72, 2019, https://doi.org/10.1109/LRA.2018.2878972.

[43] J. Lei, Z. Ge, P. Fan, W. Zou, T. Jiang, and L. Dong, "Design and Manufacture of a Flexible Pneumatic Soft Gripper," *Applied Sciences*, vol. 12, no. 13, p. 6306, 2022, https://doi.org/10.3390/app12136306.

[44] N. R. Sinatra, C. B. Teeple, D. M. Vogt, K. K. Parker, D. F. Gruber, and R. J. Wood, "Ultragentle manipulation of delicate structures using a soft robotic gripper," *Science Robotics*, vol. 4, no. 33, p. eaax5425, 2019, https://doi.org/10.1126/scirobotics.aax5425.

[45] F. Y. Wu and H. H. Asada, "Decoupled Motion Control of Wearable Robot for Rejecting Human Induced Disturbances," *2018 IEEE International Conference on Robotics and Automation (ICRA)*, pp. 4103-4110, 2018, https://doi.org/10.1109/ICRA.2018.8461109.

[46] A. S. Ciullo *et al*., "A Novel Soft Robotic Supernumerary Hand for Severely Affected Stroke Patients," *IEEE Transactions on Neural Systems and Rehabilitation Engineering*, vol. 28, no. 5, pp. 1168-1177, 2020, https://doi.org/10.1109/TNSRE.2020.2984717.

[47] I. Hussain, G. Spagnoletti, G. Salvietti, and D. Prattichizzo, "An EMG Interface for the Control of Motion and Compliance of a Supernumerary Robotic Finger," *Frontiers in Neurorobotics*, vol. 10, 2016, https://doi.org/10.3389/fnbot.2016.00018.

[48] K. Umezawa, Y. Suzuki, G. Ganesh, and Y. Miyawaki, "Bodily ownership of an independent supernumerary limb: an exploratory study," *Scientific Reports*, vol. 12, no. 1, p. 2339, 2022, https://doi.org/10.1038/s41598-022-06040-x.

[49] Z. Tang, L. Zhang, X. Chen, J. Ying, X. Wang and H. Wang, "Wearable Supernumerary Robotic Limb System Using a Hybrid Control Approach Based on Motor Imagery and Object Detection," *IEEE Transactions on Neural Systems and Rehabilitation Engineering*, vol. 30, pp. 1298-1309, 2022, https://doi.org/10.1109/TNSRE.2022.3172974.

[50] J. Guggenheim, R. Hoffman, H. Song and H. H. Asada, "Leveraging the Human Operator in the Design and Control of Supernumerary Robotic Limbs," *IEEE Robotics and Automation Letters*, vol. 5, no. 2, pp. 2177-2184, 2020, https://doi.org/10.1109/LRA.2020.2970948.

[51] X. Zhang, J. Liu, and Y. Li, "Research on Simulation System for Human-SRL Collaborative Motion Planning," *Journal of Robotics*, vol. 2022, no. 1, p. 7561891, 2022, https://doi.org/10.1155/2022/7561891.

[52] Q. Zhan *et al*., "CMM-Based Cooperative Control Strategy of Supernumerary Robotic Limbs for Human Motion," *Intelligent Robotics and Applications*, pp. 588-598, 2023, https://doi.org/10.1007/978-981-99-6498-7_50.

[53] Z. Tu, Y. Fang, Y. Leng and C. Fu, "Task-Based Human-Robot Collaboration Control of Supernumerary Robotic Limbs for Overhead Tasks," *IEEE Robotics and Automation Letters*, vol. 8, no. 8, pp. 4505-4512, 2023, https://doi.org/10.1109/LRA.2023.3285474.

[54] Z. Anvari, A. Mirhaghgoo, and Y. Salehi, "Real-time angle estimation in IMU sensors: An adaptive Kalman filter approach with forgetting factor," *Mechatronics*, vol. 106, p. 103280, 2025, https://doi.org/10.1016/j.mechatronics.2024.103280.

[55] M. Ariyanto, C. M. M. Refat, K. Hirao, and K. Morishima, "Movement Optimization for a Cyborg Cockroach in a Bounded Space Incorporating Machine Learning," *Cyborg and Bionic Systems*, vol. 4, p. 0012, 2023, https://doi.org/10.34133/cbsystems.0012.

[56] S. O. H. Madgwick, A. J. L. Harrison and R. Vaidyanathan, "Estimation of IMU and MARG orientation using a gradient descent algorithm," *2011 IEEE International Conference on Rehabilitation Robotics*, pp. 1-7, 2011, https://doi.org/10.1109/ICORR.2011.5975346.

[57] V. Guimarães, I. Sousa, and M. V. Correia, "Orientation-invariant spatio-temporal gait analysis using foot-worn inertial sensors," *Sensors*, vol. 21, no. 11, p. 3940, 2021, https://doi.org/10.3390/s21113940.

[58] J. Luo *et al*., "A Human–Robot Collaboration Control Framework for Supernumerary Robotic Limbs," *Journal of Field Robotics*, vol. 43, no. 1, pp. 34-48, 2026, https://doi.org/10.1002/rob.70025.

[59] J. Babič *et al*., "Challenges and solutions for application and wider adoption of wearable robots," *Wearable Technologies*, vol. 2, p. e14, 2021, https://doi.org/10.1017/wtc.2021.13.

[60] D. Kim *et al*., "Eyes are faster than hands: A soft wearable robot learns user intention from the egocentric view," *Science Robotics*, vol. 4, no. 26, p. eaav2949, 2019, https://doi.org/10.1126/scirobotics.aav2949.

[61] W. Huo, S. Mohammed, J. C. Moreno and Y. Amirat, "Lower Limb Wearable Robots for Assistance and Rehabilitation: A State of the Art," *IEEE Systems Journal*, vol. 10, no. 3, pp. 1068-1081, 2016, https://doi.org/10.1109/JSYST.2014.2351491.

[62] H. Xia *et al*., "Shaping high-performance wearable robots for human motor and sensory reconstruction and enhancement," *Nature Communications*, vol. 15, no. 1, p. 1760, 2024, https://doi.org/10.1038/s41467-024-46249-0.

[63] W. Wendong *et al*., "Design and verification of a human–robot interaction system for upper limb exoskeleton rehabilitation," *Medical Engineering & Physics*, vol. 79, pp. 19-25, 2020, https://doi.org/10.1016/j.medengphy.2020.01.016.

[64] J. V. Kopke, L. J. Hargrove, and M. D. Ellis, "Applying LDA-based pattern recognition to predict isometric shoulder and elbow torque generation in individuals with chronic stroke with moderate to severe motor impairment," *Journal of NeuroEngineering and Rehabilitation*, vol. 16, no. 1, p. 35, 2019, https://doi.org/10.1186/s12984-019-0504-1.

[65] B. Schabron, J. Desai, and Y. Yihun, "Wheelchair-Mounted Upper Limb Robotic Exoskeleton with Adaptive Controller for Activities of Daily Living," *Sensors*, vol. 21, no. 17, p. 5738, 2021, https://doi.org/10.3390/s21175738.